# Drude theory in Reissner-Nordström and Gubser-Rocha holographic strange metals

Moors, Ole

# Drude theory in Reissner-Nordström and Gubser-Rocha holographic strange metals

Thesis

submitted in partial fulfillment of the
requirements for the degree of

Master of Science
in
Theoretical Physics


| | |
|---|---|
| Author : | Ole Moors |
| Student ID : | 2047055 |
| Supervisor : | Prof.dr. K.E. Schalm |
| $2^{nd}$ corrector : | Prof.dr. J. Zaanen |


Leiden, The Netherlands, July 22, 2022

# Drude theory in Reissner-Nordström and Gubser-Rocha holographic strange metals

**Ole Moors**

Huygens-Lorentz Institute for Theoretical Physics, Leiden University
P.O. Box 9506, NL-2300 RA Leiden, The Netherlands

July 22, 2022

## Abstract

Since the 80s, strange metals, metals where the electrons are so densely entangled that the conventional condensed matter paradigm of Short Ranged Entanglement fails, have eluded any form of study due to the sign problem, which renders numerical calculations impossible. However, holography, a duality between strongly coupled quantum field theory problems and classical general relativity problems of one spatial dimension higher, grants us a way to circumvent the sign problem. In this thesis, we will run a modified version of code that was once used to simulate binary black holes on a supercomputer to calculate the properties of two $2+1$-dimensional holographic models for strange metals, the Reissner-Nordström metal and the Gubser-Rocha metal, subject to an ionic lattice potential: the code needed to simulate the Gubser-Rocha metal was only finished last year. We then investigate whether the DC electrical conductivity $\sigma$, thermopower $\alpha$ and thermal conductivity $\bar{\kappa}$ obey four different Drude models: one basic relativistic model and three models with different extra incoherent terms, models A, B and C. We find that model A, the most conventional model, fails, while the conductivities obey model C ($\kappa$-dominated transport) for low lattice strength $A$ and model B ($\sigma_{Q=0}$-dominated transport) for high $A$. We suspect this surprising result is caused by a pole collision causing a crossover between two regimes, but more research needs to be done to verify this.

# Contents

Chapter 1

# Introduction

For thousands of years, humans have used metals, and they have become an ever-increasingly important part of our lives. Originally, we mostly used metals to create strong tools and as sturdy building materials. However, metals gained a new role as conductors when electricity started to actively be researched from the 17th century onward. During this time, it was discovered that electric as well as heat transport are governed by conductivities relating the electric field $\vec{E}$ and the thermal gradient $\vec{\nabla}T$ on a material to electric and heat currents $\vec{J}$ and $\vec{Q}$ in the material. These can be compactly expressed in the thermoelectric conductivity matrix [1]:

$$\begin{pmatrix} \vec{J} \\ \vec{Q} \end{pmatrix} = \begin{pmatrix} \sigma & T\alpha \\ T\bar{\alpha} & T\bar{\kappa} \end{pmatrix} \begin{pmatrix} \vec{E} \\ -\frac{\vec{\nabla}T}{T} \end{pmatrix} \tag{1.1}$$

Here, $T$ is the temperature, $\sigma$ is the electrical conductivity matrix, $\bar{\kappa}$ the thermal conductivity matrix and $\alpha$ and $\bar{\alpha}$ are the thermopower matrices.

These conductivities could be measured for different metals, but the theorists were still in the dark: how did these different conductivities arise from the properties of the materials? This changed in 1897, when J. J. Thomson discovered the electron. Just three years later, in 1900, Paul Drude published the first microscopic theory of metals, which he derived from a very simple model of classical electrons colliding with positively charged scattering centers (atoms were not discovered yet) [2]. He derived the following differential equation for the average electron momentum $\langle \vec{p} \rangle$:

$$\frac{d}{dt}\langle\vec{p}\rangle = q\left(\vec{E} + \frac{\langle\vec{p}\rangle \times \vec{B}}{m}\right) - \frac{\langle\vec{p}\rangle}{\tau} \tag{1.2}$$

Here, $\vec{B}$ is the magnetic field, $q$ and $m$ are the electron charge and mass, and $\tau$ is the mean free time of the electrons between collisions with the positive charges. From this differential equation, the electrical conductivity matrix can be calculated: for example, in the case of $\vec{B} = 0$, we get for an electric field $\vec{E}(t) = \vec{E}e^{-i\omega t}$

$$\sigma(\omega) = \frac{nq^2}{m}\frac{1}{(\frac{1}{\tau} - i\omega)} \ , \tag{1.3}$$

where $n$ is the particle density. Now, if you add thermal effects to the theory, the rest of the thermoelectric conductivity matrix can be computed as well.

For a classical theory derived before the discovery of quantum mechanics and even atoms, the predictions the Drude model gives for the conductivities and related properties were shockingly accurate, reproducing known behaviour of both the DC and AC conductivity and predicting the Hall effect and magnetoresistance, the dependence of the electrical conductivity on the magnetic field. It grossly overestimated the electronic heat capacity of metals, but all in all, the Drude model was a great success. Perhaps one reason for its accuracy was that, unbeknownst to even Drude, the Drude model was secretly far more than just a theory of classical electrons. But we will discuss that later in this thesis.

Our understanding of metals once again changed drastically with the discovery of quantum mechanics. It turned out that metals are not just charged orbs bouncing of other charged orbs, but electronic wavefunctions in an atomic potential. In 1928, Arnold Sommerfeld incorporated quantum mechanics into the Drude model, creating the free electron model [3], the first quantum theory of metals. This model predicted a far more accurate value for the electronic heat capacity than the Drude model, among other things. However, the free electron model completely ignored electron-electron interactions and only took the atoms into account as periodic boundary conditions, which still gave rise to several inaccuracies.

But over the years, our understanding of the quantum nature of matter grew, and better and better models were found. It was eventually found that the theories that best described real metals were all of the same general form, with a quantum mechanical ground state of the form [4]:

$$|\Phi_{Cl}\rangle = A|\Phi^0_{Cl}\rangle + \sum_{i=2}^{N_H} a_i|\Phi_i\rangle \tag{1.4}$$

Here, $|\Phi^0_{Cl}\rangle$ is a product of single particle states and of the coefficients $A$ and $a_i$, only $A$ stays finite in the limit $N_H \to \infty$, where $N_H$ is the dimension of the Fock space. States of this form are called Short Ranged Entangled (SRE) products, and their physical meaning is as follows: the quantum mechanical ground state of SRE matter is dominantly a simple product state, allowing for a "classical" picture of the system, think of a set of determinate spins on a lattice. Effects of entanglement between particles are weak enough to be captured by perturbation theory, greatly simplifying calculations.

This paradigm of "classical condensates" encompasses a broad class of systems: things as relatively simple as crystals and as seemingly esoteric as superconducting metals all fall under it. The Fermi liquid, the definitive theory of metals proposed by Lev Landau in 1956 [5], is also a classical condensate. It supposes that interacting electrons in a metal can be described as a non-interacting Fermi gas of quasiparticles with a modified effective mass: this is the core product state. The effects of entanglement are taken into account by allowing the quasiparticles to have finite lifetimes and by allowing for fluctuations along the Fermi surface. Later on, Fermi liquid theory was generalised to include conventional Bardeen-Cooper-Schreiffer (BCS) superconductivity [6], and the theoretical description of electrons in metals seemed settled.

That is, until 1986. In that year, Bednorz and Müller discovered the alloy $Ba_xLa_{5-x}Cu_5O_{5(3-y)}$, a so-called cuprate, had a critical temperature of $T_c = 35$ K [7]. This was higher than what was generally thought at the time to be the maximum $T_c$ of a BCS superconductor. Superconductors with even higher $T_c$ were later found*, and the question arose: what mechanism governed these high-$T_c$ superconductors?

Initially, extensions of Fermi liquid theory and BCS superconductivity were considered. However, that changed when the properties of the cuprates were studied in more detail. Cuprates consist of stacked alternating layers of $CuO_2$ and an insulator, effectively creating a two-dimensional metal [9]. The copper oxide layers are normally antiferromagnetic Mott insulators, where electrons cannot move because the electrons at each lattice site strongly repel each other. However, hole dopants can be introduced in the insulator

*In fact, just one year later, it was found that replacing lanthanum with ytterbium in Ba-La-Cu-O to create Y-Ba-Cu-O increases $T_c$ to more than 80 K [8].

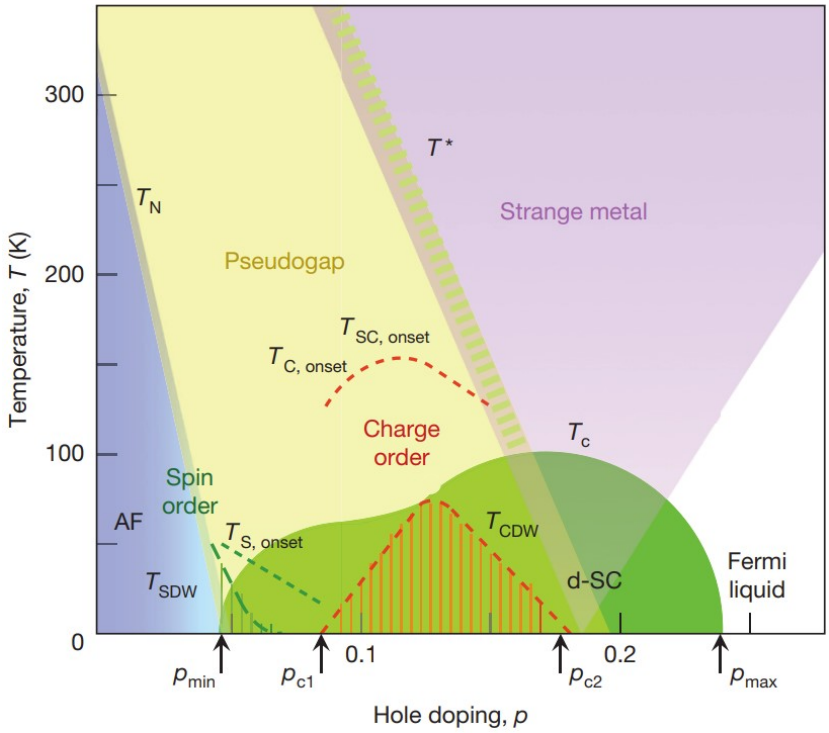


***Figure 1.1:*** *Schematic phase diagram of a cuprate as a function of temperature $T$ and hole doping level $p$, made in 2015. The blue area denotes the antiferromagnetic phase, the yellow area a pseudogap phase, the green area the (d-wave) superconducting phase, and the purple area the strange metallic phase. In the white area, the system is a regular Fermi liquid [10]. Note: it has since been found that the strange metal phase is not actually a wedge, but it has a finite width at $T = 0$, see [11].*

layers, removing electrons from the copper layers and giving the electrons more breathing room. This leads to a very rich phase space as a function of temperature and hole doping level, see Fig. 1.1 [10].

Of particular interest is the "strange metal" phase: when the transport properties of this phase were first measured, properties profoundly unlike anything expected from a Fermi liquid were found. Perhaps the most striking difference is in the resistivity. Fermi liquids are characterised by $\rho \sim T^2$ for low temperature $T$, and the resistivity saturates at the Mott-Ioffe-Regel limit when the mean free path of the quasiparticles becomes of the order of the lattice constant of the metal [12]. However, cuprates have a linear resistivity, $\rho \sim T$, that holds for all temperatures, up until the melting point of the cuprate [13]. Similar strangely simple behaviour was found when measuring

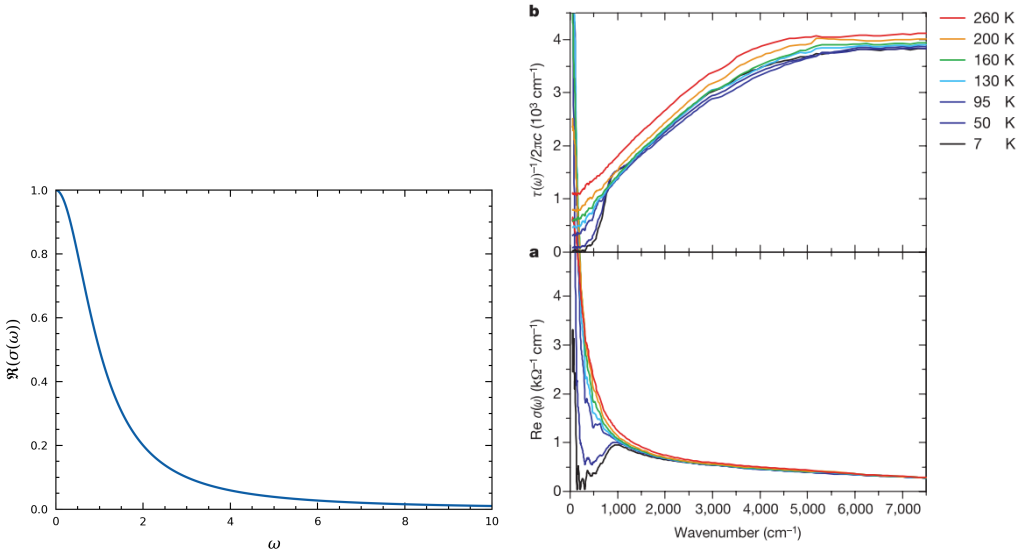


***Figure 1.2:*** *Comparison of a generic optical Drude response with* $nq^2/m = \tau = 1$ *(left) to experimental optical conductivity data measured in the cuprate* $Bi_2Sr_2Ca_{0.92}Y_{0.08}Cu_2O_{8+\delta}$ *[14] (right, bottom plane).*

the optical (AC) conductivity: as we can see in Fig. 1.2, it looks almost exactly like Drude theory[†], with a relaxation time equal to $\tau = \hbar/(k_B T)$, theorised to be the smallest possible time related to heat production [9, 14]. Other deviations from Fermi liquid theory have also been found in the temperature dependence of the Hall angle and the magnetic field dependence of the magnetoresistance [11].

As Bob Laughlin once said, a very powerful principle is needed to explain these unreasonably simple properties [15]. The claim is thus: strange metals are not actually SRE products, they are LRE (Long Ranged Entangled) systems, where the ground state has no dominant product state term, everything is entangled with everything, and even the notion of particles has disappeared. This is very interesting and exciting, but also very problematic, as we have lost the mathematical simplification that comes with the SRE paradigm. We are now dealing with fully nontrivial entangled quantum states of an immense number of particles, a NP-hard problem that could only be solved by a quantum computer. For this reason, these metals are also called "quantum supreme matter".

However, there is hope, in a mathematical result born from the pursuit of

[†]It only deviates at low temperatures because the cuprate starts to superconduct there.

string theory: holography. Holography allows us to map a maximally entangled quantum system onto a general relativistic Anti-de Sitter space of one dimension higher, and it turns out we can actually calculate things on the relativistic side with the help of a supercomputer.

In this thesis, we will use holography to calculate and study the properties of two holographic models for cuprates, the Reissner-Nördstrom metal and the Gubser-Rocha metal, and in particular, we will investigate if their conductivities obey Drude theory: this is our research question. In Chapter 2, we will discuss quantum criticality, the most well known source of LRE and perhaps its central pillar, and the sign problem, the source of the NP-hardness that prevents us from numerically simulating cuprates. In Chapter 3, we will discuss holography, and how to build and study the Reissner-Nördstrom and Gubser-Rocha metals. In Chapter 4, we will discuss some theory necessary to understand our specific research, and in particular, why we expect something as exotic as a holographic strange metal to obey simple Drude theory. In Chapter 5, we will present our results, upon which we will discuss them in Chapter 6. Finally, in Chapter 7, we will present our conclusions and give an outlook on future research.

Chapter 2

# Quantum criticality

As stated before, there are profound and fundamental computational difficulties in the quest to find a theoretical description of quantum supreme matter. But first, we must discuss what we already know about LRE systems and what forms they can take. In this chapter, we will discuss quantum criticality, the most well-known source of long range entanglement and a good example for illustrating how it works. We then cover the sign problem, the source of our computational difficulties.

This chapter will mostly be a strongly abridged version of Jan Zaanen's lecture notes on quantum supreme matter, so for a more extensive review of these topics, see [9].

## 2.1 Stoquastic systems

From statistical physics, we have a good intuition of how regular critical points in thermodynamical systems work. When two phases of a system are separated by a second-order phase transition, a critical point lies between them in phase space, where the correlation length becomes infinite and the system becomes scale invariant, the last of which causes physical quantities to submit to universal power laws and scaling relations in the neighbourhood of the critical point. Typically, these phase transitions are marked by a critical temperature (like in the Ising model), but the phase space can also depend on other parameters, like the pressure.

But it turns out that something similar can happen in a quantum system at zero temperature. As we discussed earlier, most known forms of (condensed)

matter have a ground state of the form in Eq. 1.4: the system is determined by a certain classical order, and all quantum effects come in the form of fluctuations around this order. But such systems often depend on certain parameters, such as the hole doping $p$ in the cuprates, and $|\Phi^0_{Cl}\rangle$ might not be the same for all values of those parameters: at certain points in the parameter space, the system might transition from one classical order to another. This is called a quantum phase transition, and between the phases lies a system without a dominating classical order: a quantum critical point.

As you might have guessed, quantum critical points are quantum supreme LRE systems, the most well-known kind. In general, quantum critical states differ from classical critical states in significant ways, as we will see later. However, we can start simple: in some cases, there is actually an exact mathematical correspondence between a quantum system and a statistical physics problem of one Euclidean dimension higher. The physical properties of a quantum system are given by quantum correlators, which are in turn given by the quantum partition function:

$$\mathcal{Z}_\hbar = \sum_{\text{histories}} e^{iS_{\text{history}}/\hbar} \tag{2.1}$$

Here, the sum goes over all possible histories (or paths) of the system, and $S_{\text{history}}$ is the action of the system in this particular history. This is the path integral formulation of quantum mechanics. But we can perform a so-called Wick rotation, where we replace time by imaginary time, $t \to -i\tau$, effectively making time another Euclidean coordinate by inverting its signature ($-dt^2 \to d\tau^2$). Because the action is an integral over the spacetime coordinates, and the kinetic term of the Lagrangian will transform as $(\partial_t \Psi)^2 \to -(\partial_\tau \Psi)^2$, the action transforms as $S \to iS_E$, where $S_E$ is the action in Euclidean time with kinetic and potential terms chosen with positive signs. The partition function now becomes:

$$\mathcal{Z}_\hbar = \sum_{\text{histories}} e^{-S_{\text{history},E}/\hbar} \tag{2.2}$$

But if $S_E$ is real, this is just a thermal partition function, a sum over probabilities of different configurations of a system in $d$ spatial coordinates and the Euclidean time coordinate. $S_E$ takes the role of the energy of the configurations, nicely marrying the concepts of minimising the action and minimising the energy, and $\hbar$ takes the role of temperature, which reflects the fact that quantum phase transitions are driven by quantum fluctuations instead of by

thermal fluctuations. Systems where $S_E$ is real are called stoquastic systems, and their quantum critical points are the most well-understood form of quantum supreme matter, due to their direct correspondence to classical critical points.

This correspondence gives quantum critical states in stoquastic systems a rather familiar form. Just like in thermodynamic systems, the correlation length becomes infinite at the quantum critical point and the scale invariance on the statistical physics side of the correspondence translates to conformal invariance on the quantum side, which is scale invariance combined with Poincaré invariance and invariance under so-called special conformal transformations.

Furthermore, thermal correlation functions on the statistical side of the correspondence are power laws in the Euclidean distance $r_E = \sqrt{\omega_n^2 + c^2k^2}$ at the critical point:

$$\langle \Psi(r)\Psi(0)\rangle \sim \frac{1}{r_E^{2\Delta_\Psi}} \ , \tag{2.3}$$

where $\omega_n$ is the Matsubara frequency, the Wick rotated version of the regular frequency $\omega$, and $\Delta_\Psi$ is called the conformal dimension of $\Psi$. Wick rotating back to real frequencies reveals two-point functions in the quantum critical state submit to a complex-valued brand of power laws: branch cuts. They are of the form:

$$\langle \Psi\Psi\rangle_{\vec{k},\omega} \sim \frac{1}{\left(c^2k^2 - \omega^2\right)^{d/2+1/2-\Delta_\Psi}} \tag{2.4}$$

Setting $2\Delta_\Psi = d - 1$ here, we recover the two-point function of a system of free particles, the most trivial conformally invariant system. But for $2\Delta_\Psi \neq d - 1$, this is very different from the Lorentzian poles that usually signify the presence of (quasi)particles in condensed matter systems, as the scaling dimensions become anomalous (irrational numbers): this is a manifestation of the fact that quantum critical systems do not have particles, in the usual sense.

But what about the finite temperature? In real life, quantum systems do not always live at absolute zero, after all. Through a cumulative effort by Kubo, Martin and Schwinger [16, 17], it was discovered that we can describe quantum systems at finite temperature by making the Euclidean time periodic in $\hbar/(k_BT)$, effectively making time a closed circle. At the quantum

critical point, this breaks scale invariance in the Euclidean time direction, and, at $\hbar\omega << k_BT$, the linear response functions of the system (which are just equal to the two-point functions) submit to so-called finite size scaling:

$$\chi_{\Psi,\Psi}(\omega, T) = \frac{1}{T^{\Delta_\Psi}} F_\Psi \left( \frac{\hbar\omega}{k_BT} \right) \tag{2.5}$$

They only depend on a power law in $T$ and a universal function of the $\omega/T$ ratio that is purely determined by the symmetries and dimensionality of the system. For $\hbar\omega >> k_BT$, the timescales at which the system is probed are much smaller than the period of the Euclidean time, and the system behaves as if $T = 0$.

This idea of circular time gives two more important predictions. Firstly, quantum critical systems at finite temperature have no time scales except $\hbar/(k_BT)$, the periodicity of the time circle. Now comes an important result: in a many-body system, any operator whose relaxation is determined by only one characteristic time $\tau_\Psi$ follows a Drude equation [15, 18]:

$$\frac{d\Psi}{dt} + \frac{1}{\tau_\Psi}\Psi = M_\Psi \tag{2.6}$$

Since the only time scale is $\hbar/(k_BT)$, dimensional analysis dictates $\tau_\Psi$ must be given by:

$$\tau_\Psi = A_\Psi \frac{\hbar}{k_BT} \ , \tag{2.7}$$

where $A_\Psi$ is of order 1. This is precisely the so-called Planckian dissipation seen in cuprates. We can also see why this is theorised to be the shortest possible time associated with heat production: at shorter timescales, a quantum system will not even notice it has a temperature, so anything related to heat is nonexistent at these scales. Furthermore, a result from the Drude theory of electrical transport is that $\rho \sim 1/\tau$, where $\rho$ is the resistivity and $\tau$ is the momentum relaxation time. If $\tau$ was of the form in Eq. 2.7, we would have $\rho \sim T$: this could already be a hint at the origin of the linear resistivity.

Secondly, quantum criticality is characterised by infinite correlation length and time, and when moving away from the quantum critical point, the correlation time will decrease as a power law in the parameters relevant to the phase transition. But if time is periodic and the correlation time is longer

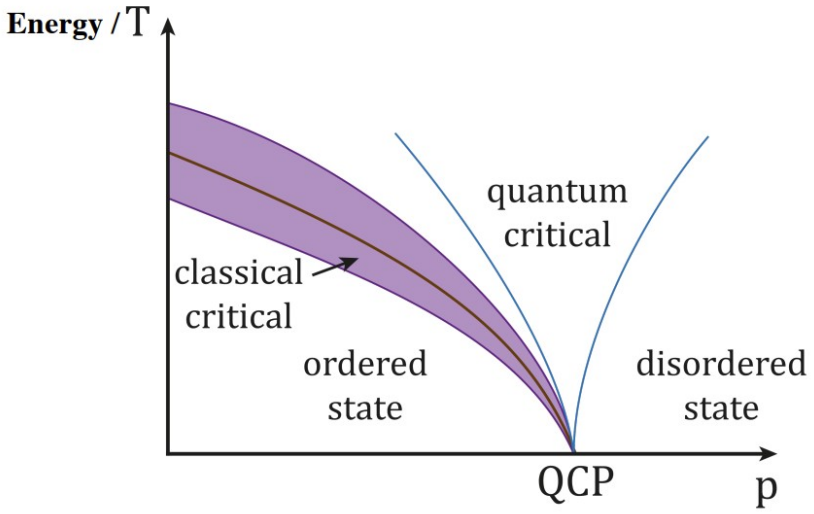


***Figure 2.1:*** *Schematic phase diagram in temperature $T$ and another parameter $p$, showing both a line of classical critical points and a quantum critical wedge rooted in a quantum critical point $p_c$. The sides of the wedge follow a power law in the reduced parameter, $T_c \sim \left(\frac{p-p_c}{p_c}\right)^{\alpha}$. [9]*

than the period, the periodicity will force an effective infinite correlation time. The correlation length follows suit due to Lorentz invariance, and it turns out quantum criticality also manifests *around* the quantum critical point at finite temperature, not just directly at the critical point. This results in a "quantum critcal wedge" in the phase space. Its form is illustrated in Fig. 2.1, compared to a line of classical thermal critical points.

As can be seen in Fig. 1.1, it was thought in 2015 that the strange metal phase in cuprates was such a quantum critical wedge. This was a rather attractive idea, considering the measured Planckian dissipation and power law form of the sides of the phase. However, it was later discovered that the strange metal phase is not rooted in a single point at $T = 0$, but the width of the phase is still finite there [11]. The story is just not quite this simple for cuprates, and we will come to appreciate this later.

## 2.2 The sign problem

We have been able to derive the results so far by using the direct correspondence between many-body quantum systems and statistical systems given by Eqs. 2.1 and 2.2. This works great for systems where $S_E$ is real, which is

most typically the case for bosonic systems. However, this all goes terribly wrong when $S_E$ becomes complex: we get a statistical system with negative or even complex probabilities, which makes no sense. This tends to happen for fermionic systems, which strange metals, just like all metallic states, sadly fall under.

Let us illustrate how this happens and why it is a problem. Consider a system with $N$ particles with mass $M$ at temperature $T$ where the dynamics in Euclidean time are described by the action:

$$\mathcal{S}[\mathbf{R}] = \int_0^{\hbar\beta} d\tau \left( \frac{M}{2} \dot{\mathbf{R}}^2(\tau) + V(\mathbf{R}(\tau)) \right) \tag{2.8}$$

Here, $\beta = 1/(k_B T)$ as usual, and $\mathbf{R} = (\vec{r}_1, \cdots, \vec{r}_N)$ are the positions of the particles. For distinguishable particles, we can now find the canonical partition function of the system using Eq. 2.2:

$$\mathcal{Z} = \int \mathrm{d}\mathbf{R} \rho(\mathbf{R}, \mathbf{R}; \beta) \ , \tag{2.9}$$

where:

$$\rho_D \left( \mathbf{R}, \mathbf{R}'; \beta \right) = \int_{\mathbf{R} \to \mathbf{R}'} \mathcal{D}\mathbf{R} \exp(-\mathcal{S}[\mathbf{R}] / \hbar) \tag{2.10}$$

In total, this expression integrates over all possible paths the particles can take: the integral in Eq. 2.9 goes over all possible sets of particle coordinates, and the one in Eq. 2.10 goes over all possible paths the particles can take from $\mathbf{R}$ to $\mathbf{R}'$. Due to the periodicity of Euclidean time, all particles need to begin and end at the same point... that is, if the particles are distinguishable. If the particles are bosons or fermions, their "worldlines" can end at each others starting points, and we need to replace $\rho_D \left( \mathbf{R}, \mathbf{R}'; \beta \right)$ in Eq. 2.9 by a symmetrised or antisymmetrised version, respectively:

$$\rho_{B/F}(\mathbf{R}, \mathbf{R}; \beta) = \frac{1}{N!} \sum_{\mathcal{P}} (\pm 1)^p \rho_D(\mathbf{R}, \mathcal{P}\mathbf{R}; \beta) \ , \tag{2.11}$$

where we sum over all permutations of the particle coordinates, and $p$ is the sign of the permutation. The plus sign is for bosons, the minus sign for fermions.

What these permutation terms look like is illustrated in Fig. 2.2 for three particles in one spatial dimension. The worldlines essentially form "polymers" that wrap around a Euclidean time cylinder with circumference $\hbar/(k_B T)$, and whose energy is given by $\frac{M}{2}\dot{\mathbf{R}}^2(\tau) + V(\mathbf{R}(\tau))$. If the worldline of a particle ends at the start of the worldline of another particle, they will join into one polymer that wraps multiple times around the cylinder: in the case of the figure, all the particles have joined into a single polymer.

When the particles are free, so $V(\mathbf{R}(\tau)) = 0$, the properties of the system become familiar. If we fix the chemical potential $\mu$ instead of $N$ and transform to the grand canonical partition function:

$$Z_G(\beta, \mu) = \sum_{N=0}^{\infty} Z_{B/F}^{(N)}(\beta) e^{\beta \mu N} \ , \tag{2.12}$$

we can use some combinatorics for both bosons and fermions to recover the expressions for the average number of particles and energy we would find using the Bose-Einstein distribution and the Fermi-Dirac distribution, respectively [19]. But when interaction terms and/or external potentials are present in the Lagrangian, we can no longer find an analytical expression for the partition function. In the case of bosons, however, there has been considerable numerical success using path integral Monte Carlo methods. For example, David Ceperley managed to numerically simulate superfluidity and Bose condensation in Helium-4 to great accuracy in 1995 [20].

However, in the case of fermions, this all goes very wrong. In general, when potentials are present in a fermionic system, the alternating sum in Eq. 2.11 becomes immensely difficult to calculate for large $N$. Even numerically, the difficulties are far greater than for bosons. Numerics do not play well with alternating sums, for the same reason a rapidly oscillating sine function is harder to analyse numerically than an increasing function: numerical inaccuracies blow up during your calculations.

This is the sign problem, and it is fundamental. In 2005, Matthias Troyer and Uwe-Jens Wiese showed that, in general, the sign problem is almost certainly NP-hard (nondeterministic polynomial hard) [21], which means that the computation time increases exponentially in the number of particles, and the problem most likely cannot be solved by classical computers (if you manage to find a way, you'll probably get a Nobel prize).

So unless there is some mathematical coincidence or trick available to greatly simplify the math, you're out of luck - and this is precisely the case in

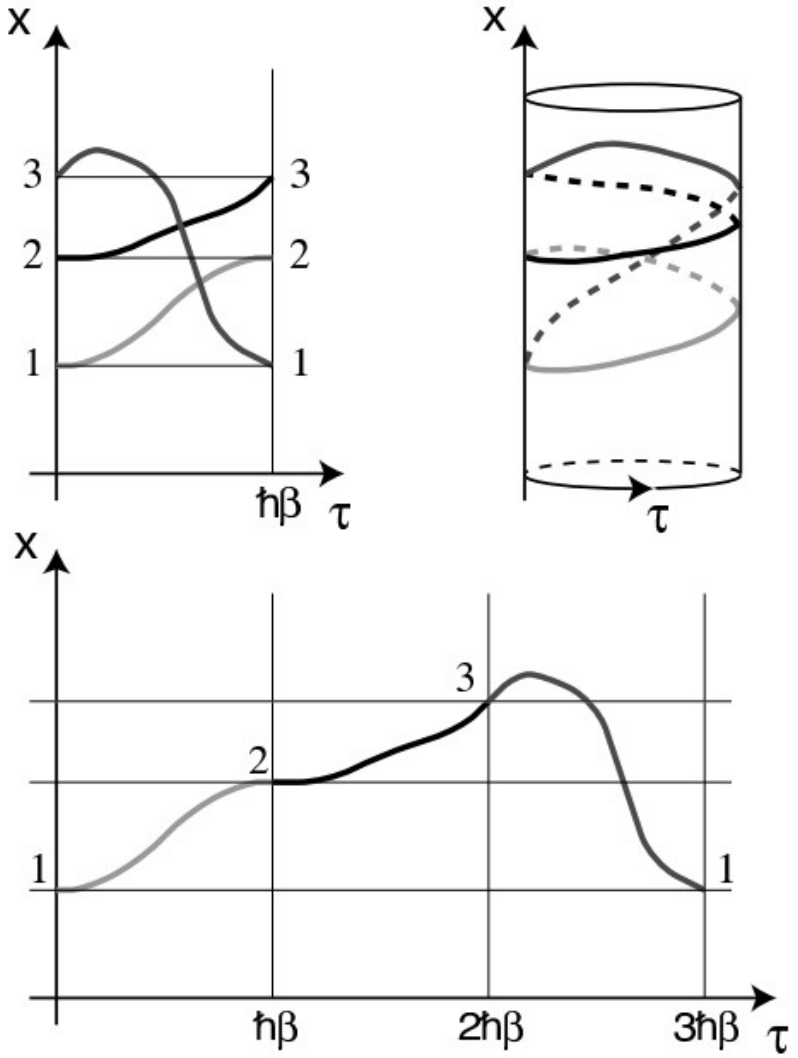


***Figure 2.2:*** *Three different ways of sketching the worldlines of three indistinguishable particles in Euclidean time at finite temperature in one spatial dimension, where the worldlines of each particle end at the start of the worldline of another particle. The top left sketch shows a single Euclidean time period, the $\tau$ axis is cylindrically wrapped up in the top right sketch, and the bottom sketch shows the full period of the worldlines. [19]*

fermionic LRE quantum systems, where the SRE paradigm of Eq. 1.4 fails. We now have only two options: we either hope a future quantum computer can crack open the NP-hardness of the problem, or we find a new mathematical trick that does work for LRE systems. As we will see in the next chapter, the latter option might be the way to go.

Chapter 3

# Holography

In an unlikely corner of physics, string theory, a way to circumvent the sign problem for fermionic LRE systems might have been found: holography. In this chapter, we will discuss the AdS/CFT correspondence, the backbone of holography, and how we can use holography to map LRE fermionic systems onto a "dual" description that we know how to work with. At the end of the chapter, we will describe two possible holographic models for cuprates, the Reissner-Nordström and Gubser-Rocha metals.

## 3.1 The AdS/CFT correspondence

On the first day of the new year in 1998, around the second superstring revolution, Juan Maldacena published a paper where he derived a theorem that can be stated as such [9, 22]:

> Maximally supersymmetric $\mathcal{N} = 4$ Yang-Mills in $D = 4$ space-time dimensions in the large $N$ limit for infinite 't Hooft coupling is dual to classical supergravity on $\mathrm{AdS}_5 \times \mathrm{S}^5$.

This is a very specific, technical theorem with a lot of string theory jargon, but after the efforts of Edward Witten [23]* and others, the high energy community came to a far more general conjecture:

*Witten's article was even published right after Maldacena's in the very same journal edition.

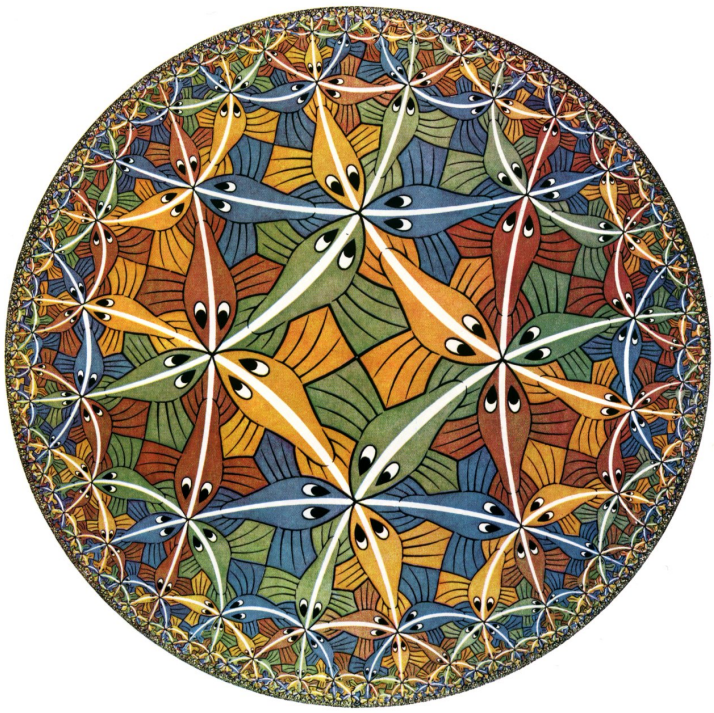

***Figure 3.1:*** *Escher's woodcut Circle Limit III, made in 1959.*

> Strongly coupled $d+1$-dimensional conformal field theories (CFT) are dual to classical general relativistic gravity in $d+2$-dimensional Anti-de Sitter (AdS) space.

Conformal field theories are simply quantum field theories that are conformally invariant, while Anti-de Sitter space is hyperbolic spacetime, with a negative cosmological constant, given by the metric [18]:

$$ds^2_{\text{AdS}} = \frac{r^2}{L^2}\eta_{\mu\nu}dx^\mu dx^\nu + \frac{L^2}{r^2}dr^2 \tag{3.1}$$

Here, $L$ is called the AdS radius. AdS space has strange properties: the distance between its center at $r = 0$ and its edge at $r = \infty$ is infinite, but one can travel between the center and edge in finite time. An intuition of how this is possible can be gained from a woodcut made by Escher in 1959, given in Fig. 3.1. There is an infinite number of fish between the center and the edge, but because they get increasingly smaller, the travel time between them ends up being finite.

The third aspect of the AdS/CFT correspondence is a very important word:

"dual". There is a duality in a physical theory if two seemingly different physical viewpoints of the theory are both correct. The most well-known duality is the wave-particle duality, where particles in quantum mechanics can also be described as waves, and the two viewpoints are connected by the Fourier transformation.

However, the duality in the AdS/CFT correspondence is special in two different ways. Firstly, it is a strong-weak duality: it is a duality between a strongly-coupled theory (the CFT) and a weakly coupled theory (classical GR gravity in AdS space, where quantum gravity is negligible). A well known example of a strong-weak duality is the Kramers-Wannier duality [24], a duality between the ordered low-temperature and the disordered high-temperature phases of the 2D square lattice Ising model: it turns out the disordered side can be described by an ordered Ising model with inverted coupling $\beta J \to 1/(\beta J)$. It is a strange idea: a disordered system turns out to actually be ordered from another point of view.

Secondly, the AdS/CFT correspondence is a holographic duality: the theories that are dual to each other differ by a dimension. Just like how a 3D hologram can be projected from a 2D surface, the AdS space can also be described as a CFT with one less dimension. Indeed, the coordinates $x^\mu$ in the AdS space directly correspond to the spacetime coordinates in the CFT, but the coordinate $r$ seems to be an extra. How does it correspond to the CFT?

It turns out that $r$ corresponds to the renormalisation scale of the CFT. If we change coordinates to $z = L^2/r$, the metric becomes:

$$ds^2_{\text{AdS}} = \frac{L^2}{z^2}\left(\eta_{\mu\nu}dx^\mu dx^\nu + dz^2\right) \tag{3.2}$$

Now, $z$ can be interpreted as the length scale at which we view the CFT. The CFT directly corresponds with the spacetime surface at $z = 0$: this surface is also called the boundary, or the ultraviolet (UV). As we increase $z$, we encounter surfaces at constant $z$ that correspond to increasingly coarse-grained versions of the CFT. As the length scale increases, more and more details are integrated out. The form of the metric is compatible with this view: the induced metric on surfaces at constant $z$ is simply proportional to the Minkowski metric, and all lengths rescale as $z$ increases. The area with $z > 0$ is also called the bulk. Finally, the area around the center of the AdS space, at large $z$, is also called the infrared (IR).

This process of renormalisation is very similar to how it is done in statistical physics (i.e., in the Ising model, we average blocks of spins into one spin als

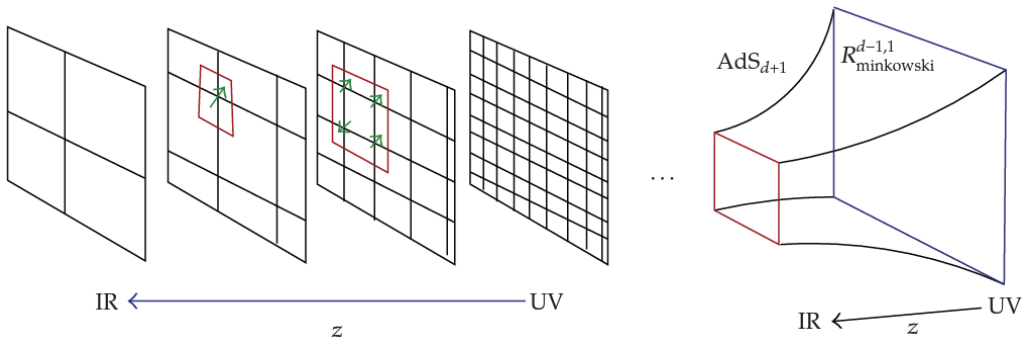


***Figure 3.2:*** *Illustration of the renormailsation process as we go from the UV to the IR. As we view the system from larger and larger scales, we integrate out more and more details, such as in the Ising model, where we average blocks of spins into one spin. [25]*

we increase the length scale), and it is illustrated in Fig. 3.2. In Fig. 3.1, we also already see how a concept of coarse-graining arises naturally in AdS space: at the boundary, there are infinitely many small fishes, while at the center, there are only a few very large fishes.

We can also describe the renormalisation in terms of $r$, where the UV and the deep IR lie at $r = \infty$ and $r = 0$, respectively. $r$ can be interpreted as the energy scale at which we probe the CFT, which is a more natural way to describe renormalisation in quantum field theory (at low energies, physics at higher energies becomes hidden or suppressed). For this reason, and because it is more intuitive to have the radial coordinate increase as we go from the center to the boundary of the AdS space, we will use $r$ as our radial coordinate from now on.

But all of this also reveals one of the backbones of the AdS/CFT correspondence: isometries in the bulk correspond to symmetries in the boundary. This is because isometries in the bulk are transformations that leave the metric invariant, and since the physics in the boundary is encoded in the bulk metric, the induced transformation on the boundary should leave its physics invariant. In fact, the statement can be made even more specific: local isometries correspond to global symmetries [18].

This is, in fact, the reason why CFTs should correspond to AdS space. As we can see in Eq. 3.1, the AdS metric is invariant under the transformation $x^\mu \to \lambda x^\mu$, $r \to r/\lambda$. But in terms of the boundary theory, this is a scale transformation, so the fact that the bulk is given by an AdS metric implies the boundary theory should be scale invariant. Using other isometries in the

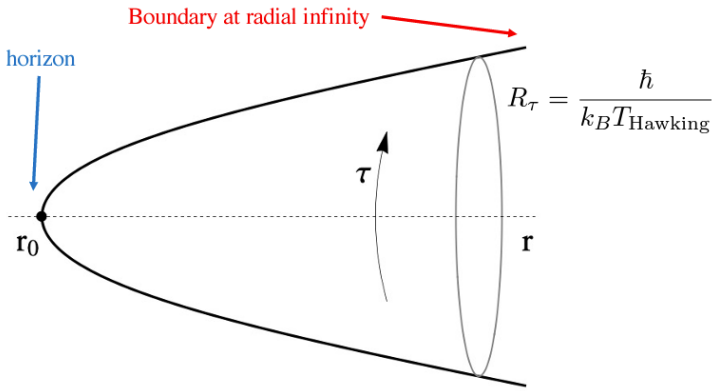


***Figure 3.3:*** *Sketch of the behaviour of the Euclidean time coordinate $\tau$ in an AdS Schwarzschild metric as we increase the radial coordinate $r$. [9]*

metric (such as Poincaré invariance), it can then further be derived that the boundary must be conformally invariant.

This correspondence between symmetries and isometries now also allows us to include temperature in our system. After all, as we established in the previous chapter, a temperature $T$ manifests in many-body quantum systems as a periodicity of the Euclidean time $\tau$ in $\hbar/(k_B T)$, and this is a symmetry. How do we include the corresponding isometry in the bulk?

The rather wild-sounding answer is: we must include a Schwarzschild black hole centered at $r = 0$! This is because, if we Wick rotate the time coordinate in the AdS Schwarzschild metric, it turns out that the black hole imposes an $r$-dependent periodicity on $\tau$, as illustrated in Fig. 3.3 [9]. At the black hole horizon, the Euclidean time dimension is completely wrapped up in an infinitesimally small period, but it expands outward as $r$ increases, gaining a period $\hbar/(k_B T_{\text{Hawking}})$ at the boundary, where $T_{\text{Hawking}}$ is the famous Hawking temperature of the black hole related to Hawking radiation.

This is a striking result: the strange notion of black hole temperature discovered by Hawking in 1974 [26] may be directly connected to temperature in solids! There is even more to this story, as the black hole also grants the system an entropy proportional to the horizon area of the black hole via the Bekenstein-Hawking formula [27]. From the GR perspective, this scaling has always been odd, since we expect the entropy of a system to roughly scale with its volume. But since the dimension of the area of the black hole is the same as that of the volume of the boundary theory, the entropy turns out to have a much more natural scaling behaviour when seen from the CFT side. The statement that black holes behave as if they have a redundant dimension

suddenly gains an intriguing meaning here.

There are many more such correspondences between bulk and boundary phenomena, and they are given by holography's counterpart of the Fourier transformation, the Gubser-Klebanov-Polyakov-Witten (GKPW) master rule [9, 23, 28]:

$$\left\langle e^{\int d^{d+1}xJ(x)O(x)} \right\rangle_{CFT} = \int \mathcal{D}\phi e^{iS_{\text{bulk}}\ (\phi(x,r))|_{\phi(x,r=\infty)=J(x)}} \tag{3.3}$$

It arises from insisting that both sides of the correspondence have equal partition functions [18]. The left hand side pertains to the CFT in the boundary. It's the generating functional of the operator $O(x)$ with source $J(x)$, and it can be used to calculate the correlators of $O$, from which the properties of the CFT can be derived.

The right hand side is part of the quantum partition function in the bulk, where we integrate over possible configurations of the field $\phi(x, r)$ dual to $O(x)$. There is, however, one condition on these configurations: $\phi(x, r)$ must match $J(x)$ at the boundary. In general, calculating the right hand side requires knowledge of quantum gravity, but when the CFT is strongly coupled, the partition function enters the classical limit and only the configuration that minimises the action contributes, which we know how to find in GR.

A basic result of the GKPW rule is derived in [29], and we'll sketch it here. We put a massive scalar field $\phi$ in the AdS bulk without a black hole using the action:

$$\mathcal{S} = -\frac{1}{2}\int d^{d+2}x\sqrt{-g}\left[g^{MN}\partial_M\phi\partial_N\phi + m^2\phi^2\right] \tag{3.4}$$

After finding the equations of motion and solving them, it can be found that $\phi(x, r)$ takes the following asymptotic form at the boundary ($r \to \infty$):

$$\phi(x, r) \sim A(x)r^{\Delta-d-1} + B(x)r^{-\Delta} \tag{3.5}$$

Here, $d + 1$ is the dimension of the boundary (so $d$ spatial dimensions) and:

$$\Delta = \frac{d+1}{2} + \sqrt{\frac{(d+1)^2}{4} + m^2L^2} \tag{3.6}$$

Using the GKPW rule in the case of classical gravity, we can now find that the two point function of the operator $O$ dual to $\phi$ takes the momentum space form:

$$\langle O(k)O(-k)\rangle \sim \frac{B(k)}{A(k)} \tag{3.7}$$

These results have a physical interpretation. $A$ is the coefficient of the leading term in $\phi(x,r)$ at the boundary, since that term has the largest power of $r$: this must mean $A$ corresponds to the source of $O$ by the GKPW rule. Furthermore, since the two-point function of $O$ determines the relative strength of its response to its source, $B$, the coefficient of the subleading term of $\phi(x,r)$, must correspond to the absolute response of $O$ to the source $A$, also called its vacuum eigenvalue (VEV). These arguments are very generic: in general, the leading term of a bulk field for high $r$ corresponds to the source of its dual boundary operator, and the subleading therm corresponds its response.

Furthermore, in this specific example, it can be found that:

$$\langle O(x)O(0)\rangle \sim k^{2\Delta-d-1} \tag{3.8}$$

This is just the branch cut from Eq. 2.4! $m = 0$ now gives the free theory, while $m \neq 0$ gives a quantum critical response with anomalous dimensions. This is a great indication that we're on the right track.

The large collection of dualities that can be derived from the GKPW rule are also called the dictionary, and some of its most important entries can be found in Table 3.1 [18]. Not all of them are directly relevant to this thesis, but of particular interest is the entry about the chemical potential and charge density: we will need it in the next section.

## 3.2 Finite density

We have made great progress into the world of holography so far: we now have a duality between conformal field theories at finite temperature and AdS spaces with black holes. But we are not even close to studying metals yet, all boundaries we can create are still firmly stoquastic. We need to add fermionic charge to the system, and we can see how to do this in Table 3.1: we need to include an electromagnetic vector potential in the bulk, or in other words, we need to put charge in it.

| Boundary: QFT | Bulk: GR |
|---|---|
| Partition function | Partition function |
| Scalar operator $O$ | Scalar field $\phi$ |
| Fermionic operator $O_\psi$ | Dirac field $\psi$ |
| Source of operator | Boundary value/leading coefficient of field |
| VEV of operator | Subleading coefficient of field |
| Conformal dimension of operator | Mass of field |
| Spin/charge of operator | Spin/charge of field |
| Energy-momentum tensor $T^{\mu\nu}$ | Metric $g_{\mu\nu}$ |
| Noether current $J^\mu$ | Maxwell field $A_\mu$ |
| Two-point function | Ratio of subleading and leading field coefficients |
| Renormalisation group flow | Evolution in the radial AdS direction |
| Number of degrees of freedom | AdS radius |
| Global spacetime symmetry | Local isometry |
| Global internal symmetry | Local gauge symmetry |
| Temperature | Black hole Hawking temperature |
| Chemical potential/charge density | Boundary value of electrostatic potential $A_t$ |
| Free energy | Minimised action |
| Entropy | Area of black hole horizon |

***Table 3.1:*** *Several important dualities in the dictionary of the AdS/CFT correspondence. [18]*

### 3.2.1 The Reissner-Nordström metal

The simplest way to include charge in the bulk is to impose the AdS Einstein-Maxwell (EM) action on it [18]:

$$S_{EM} = \frac{1}{16\pi G}\int d^{d+2}x\sqrt{-g}\left(R + \frac{d(d+1)}{L^2} - \frac{1}{4e^2}F_{\mu\nu}F^{\mu\nu}\right) \tag{3.9}$$

The only stationary solution[†] to this action is the Reissner-Nordström (RN) black hole metric with mass $M$ and charge $Q$:

$$ds^2_{RN} = \frac{r^2}{L^2}(-f(r)dt^2 + dx^2) + \frac{L^2}{r^2 f(r)}dr^2 \tag{3.10}$$

Here, $f(r)$ is the emblackening factor:

$$f(r) = 1 + \frac{Q^2}{r^{2d}} - \frac{M}{r^{d+1}} \tag{3.11}$$

Furthermore, the electrostatic potential $A_t$ becomes:

$$A_t = \mu\left(1 - \frac{r_0^{d-1}}{r^{d-1}}\right) \ , \tag{3.12}$$

where $\mu$ and $r_0$ are determined by $M$ and $Q$. $\mu$ is the boundary value of $A_t$, and it directly corresponds to the fermionic charge density in the boundary: it actually takes on a somewhat similar role there to that of the Fermi energy in the Fermi liquid. Finite temperature is automatically accounted for, it is once again determined by the Hawking temperature of the RN black hole.

Now that we have a finite density boundary, we finally have a system where we can circumvent the sign problem using holography! We call the boundary the Reissner-Nordström metal, and deeply strange properties can already be seen by simply studying its bulk metric. Very close to the black hole horizon, the metric asymptotically becomes $\mathrm{AdS}_2\times\mathrm{R}^d$ [9]. This refers to the fact that the spatial dimensions have become flat, and only the time and radial dimensions form an $\mathrm{AdS}_2$ subspace together.

This has a very deep consequence for the RN metal. Conformal invariance in the boundary rests on the bulk being AdS space, so at very large scales,

[†]We need the bulk metric to be stationary to have the boundary be in equilibrium.

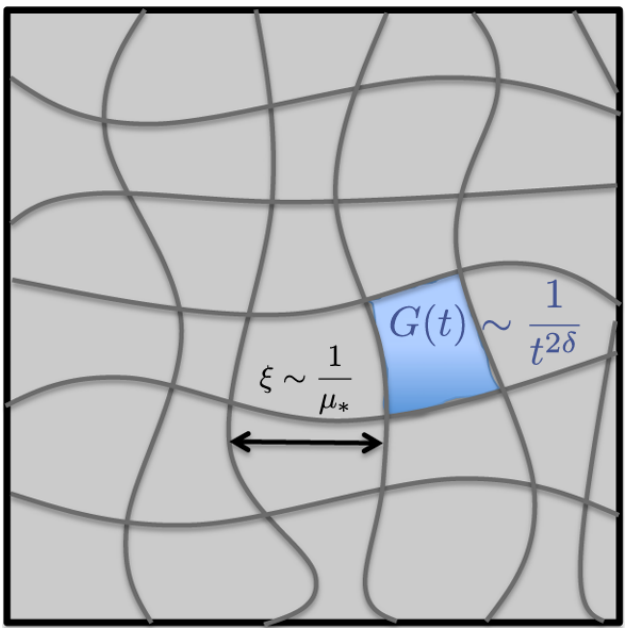


***Figure 3.4:*** *Sketch of the division of the Reissner-Nordström metal in uncorrelated patches of quantum critical matter of size $\xi \sim 1/\mu$. As shown, the temporal correlation function is still a power law. [31]*

the RN metal will have an infinite correlation time but a finite correlation length! It is as if only the time direction is quantum critical, and for this reason, this phenomenon is called local quantum criticality.

It has actually been observed in real cuprates [30], and Hong Liu and his already investigated it in a holographic context in 2012 [31]. It turns out that the spatial correlation is broken at large scales because areas in the boundary at larger distances than $\xi \sim 1/\mu$ cease to be causally connected when an RN black hole is introduced: the light cones do not overlap. As a result, the RN metal consists of patches of size $\xi$ that each behave quantum critically but do not correlate with each other, as illustrated in Fig. 3.4. This causes the electrons in the metal to behave like a hydrodynamical fluid at large scales: we will discuss that a bit more later on.

Much research has already been done into the RN metal, not least of which by former MSc students in Koenraad Schalm and Jan Zaanen's team, Martijn Janse [32] and Sam Arend [33]. However, the RN metal has a critical pathology. The RN black hole has a finite area at zero temperature due to the energy of its electric field [18], but this translates to a finite zero temperature entropy in the boundary. This is considered to be deeply unphysical,

since it requires the RN metal to have a degenerate ground energy, which is only possible in reality with an unrealistic amount of fine-tuning (any small outside influence will lift the degeneracy).

So it seems the RN is still not good enough as a model for real-life cuprates. It seems we need to add something more to the bulk, but what?

### 3.2.2 The Gubser-Rocha metal

It turns out that we have to go back to the basics to find the answer: we need to look at the string-theoretical origins of holography. Even if we work in the classical limit, the bulk still needs to ultimately answer to string theory. String theory requires several extra rolled-up (Kaluza-Klein compactified) dimensions, and those lead to a scalar field known as the dilaton [34, 35]. Including a dilaton field $\Phi$ in the bulk alongside the electromagnetism we need for finite density gives the Einstein-Maxwell-Dilaton (EMD) action [9]:

$$S_{EMD} = \frac{1}{16\pi G}\int d^{d+2}x\sqrt{-g} \times \left(R - \frac{3}{2}(\partial_\mu\Phi)^2 + \frac{6}{L^2}V(\Phi) - \frac{Z(\Phi)}{4e^2}F_{\mu\nu}F^{\mu\nu}\right) \quad (3.13)$$

Goutéraux and Kiritsis have found that, in the deep IR, the metric derived from this action takes the general form [9, 36]:

$$ds^2_{\text{EMD}} = \frac{1}{r^2}\left(-\frac{dt^2}{r^{2d(z-1)(d-\theta)}} + dx^2 + r^{2\theta/(d-\theta)}dr^2\right) \quad (3.14)$$

Here, $z$ and $\theta$ are determined by the form of the potentials $V(\Phi)$ and $Z(\Phi)$ in the action, and they have specific physical meanings. $z$ is called the dynamical critical exponent, and it determines how the correlation time and length of the system scale with respect to each other: $t \sim l^z$. We have $z = 1$ in regular CFTs due to Lorentz invariance, and $z \to \infty$ corresponds to local quantum criticality.

$\theta$ is called the hyperscaling violation coefficient, and it has the effect of altering the number of degrees of freedom "felt" by the thermodynamics: the free energy scales with the length of the system as $F \sim L^{d-\theta}$, where $\theta = 0$ gives the scaling relation called hyperscaling, hence the name of $\theta$. Another interesting feature is that a finite $\theta$ breaks the scale invariance of the bulk

metric. It can be found that, under a scale transformation $x \to \Lambda x$, the deep IR EMD metric transforms as [9]:

$$ds^2_{\text{EMD}} \to \Lambda^{2\theta/d} ds^2_{\text{EMD}} \tag{3.15}$$

The bulk metric is no longer scale invariant, but scale covariant, which means that the boundary is fundamentally no longer a CFT. This result was first discovered by Davison, Gentle and Goutéraux only three years ago, in 2019 [37]. It shows how far we have come: we have already taken holography far beyond the simple AdS/CFT correspondence.

Now, it can be found using the GKPW rule that the entropy of the system scales as [9]:

$$S \sim T^{(d-\theta)/z} \tag{3.16}$$

Using this, we can find which choice of $z$ and $\theta$ should correspond to real cuprates. As we addressed earlier, local quantum critical behaviour is measured in cuprates, which means $z \to \infty$. This, however, immediately leads to the unphysical zero temperature entropy of the RN metal... unless we also take $\theta \to -\infty$![‡] It is still unknown what $\theta \to -\infty$ means physically (an infinite number of thermodynamical degrees of freedom?), but by taking $z \to \infty$ and $\theta \to -\infty$ while keeping their ratio finite, we can remove the zero temperature entropy while preserving local quantum criticality!

Now we just need to find the value of the $\theta/z$ ratio. It turns out we need to look more closely at the holographic duality. For the RN metal, we simply introduced a classical bulk and derived a boundary from it, but we did not check if all this made sense in full quantum gravitational string theory, which is necessary for the boundary to be a physically realisable theory. For the EMD bulk action with $z \to \infty$ and $\theta \to -\infty$, Gubser and Rocha first derived for three spatial dimensions ($d = 3$) that we can get a match with string theory if $\theta/z = -1$ [38], which corresponds to taking the potentials $V(\Phi) = \cosh \Phi$ and $Z(\Phi) = e^{\Phi}$ in Eq. 3.13 [39]. The entropy now becomes:

$$S \sim T \tag{3.17}$$

This linear in $T$ entropy is called Sommerfeld entropy, and it has also been measured in real cuprates [9]. So we now have a boundary that is supported

[‡] $\theta \to \infty$ cannot happen, since $\theta > d$ leads to unphysical behaviour of the free energy.

by rigorous holography, displays local quantum criticality, and has an entropy that matches what is measured in cuprates: this all looks much better than the pathological RN metal. We call the metal in the boundary of this bulk the Gubser-Rocha (GR)[§] metal.

Interestingly, Sommerfeld entropy is normally a hallmark of Fermi liquids: this is one of the reasons why many physicists have tried to interpret cuprates as Fermi liquids for so long. This similarity might not be a coincidence. $z$ and $\theta$ are not just EMD parameters, they can be defined for a much larger variety of many-body systems using $t \sim l^z$ and $F \sim L^{d-\theta}$ as mentioned before. For a Fermi liquid in $d$ space dimensions, it can be found that $z = 1$ and $\theta = d - 1$ (the influence of the Pauli principle and the Fermi surface severely restricts the number of degrees of freedom) [9]. But this means the entropy scaling of Fermi liquids is also given by Eq. 3.16!

There is more, however. It can be found that the charge susceptibility of a general EMD boundary metal in the regime $T < \omega << \mu$ is given by [40]:

$$\mathrm{Im}\,\chi_{\mathrm{inc}}\,(\mathbf{q},\omega) = \omega^{(d-2-\theta+z)/z} F\left(\frac{\omega}{|q|^z}\right) \tag{3.18}$$

Now, taking $z = 1$, $\theta = d-1$ and $F\left(\frac{\omega}{|q|}\right) = \frac{\omega}{|q|}$ gives the charge susceptibility of the Fermi liquid in the regime $T < \omega << E_F$, where $E_F$ is the Fermi energy:

$$\mathrm{Im}\,\chi_{\mathrm{Fermi}}(\mathbf{q},\omega) = \frac{\omega}{|q|} \tag{3.19}$$

The EMD boundaries appear to behave somewhat like a Fermi liquid, except the scaling dimensions of the system have become anomalous, as we have seen before in quantum critical stoquastic systems. A possible interpretation is thus [9, 15] that cuprates are a generalised form of Fermi liquids, mixed with quantum critical-like properties. In a way, we have come full circle: the strange metals might have just been Fermi liquids all along, except with a quantum critical twist no one in the 80s could have expected.

[§]Alternatively, this can be read as "General Relativity metal", which is also quite accurate.

Chapter 4

# Methods

We have now covered the most essential parts of the theoretical background behind the use of holography to study long ranged entangled matter. We will now describe the theory specific to our research and how we gained our results. We will also explain why we will try to use Drude theory to describe transport in strange metals, and how we will try to match our data to three different possible variations of relativistic Drude theory.

## 4.1 The ionic lattice

With the holographic RN and GR metals, we have a strong basis for modelling cuprates. But we are still missing a crucial ingredient: translational symmetry breaking (TSB). Without TSB, the conductivities of our metals are all infinite: after all, translational symmetry implies momentum conservation, so applying an electric field or a thermal gradient to an infinitely long piece of metal just makes the charge accelerate forever and the electric and thermal currents approach infinity.

Translational symmetry can broken in the boundary in ways that are still analytically tractable. For example, it can be done by including a massive scalar field [41] or axions [42]. But such models are rather artificial, there is no guarantee that they have much to do with real-life cuprates. This is why, for our research, we break translational symmetry in a more realistic way: we impose an explicit periodic ionic potential on the boundary, just like how translational symmetry is broken in real metals.

We will do this by working in $2+1$ dimensions (since cuprates are 2D sys-

tems) and modulating the chemical potential in the boundary in the following way:

$$\mu(x, y) = \mu_0 \left(1 + \frac{A}{2\mu_0}(\cos(Gx) + \cos(Gy))\right) \tag{4.1}$$

This introduces two new parameters: $A$, the strength of the potential, and $G$, the wavevector of the potential. $A$ mostly controls the strength of the TSB, and we expect it to be rather large compared to $\mu^*$ in cuprates. After all, the long ranged entanglement needs to be caused by some sort of strong coupling, and Jonah Post has shown in his thesis [43] that large $A/\mu$ gives the right order of magnitude for the resistivity, supporting this view. The size of $G$ with respect to $\mu$ plays a large, qualitative role in the properties of the holographic metal, and we will talk more about it later in this chapter.

But if the ionic lattice is a so much more realistic way to break translational symmetry breaking, one might wonder why the less realistic methods are used much more often. This is because there is a large practical problem with this method: modulating the chemical potential like this destroys virtually all symmetry in the bulk, making the Einstein equations there a nightmarish system of six coupled nonlinear partial differential equations. These have no analytical solution and they are immensely hard to compute numerically. In fact, even this was not possible for a long time.

However, our team in Leiden has managed to develop code that can solve these equations. It does not have an official name, but we will call it the HoloCode. It uses the Portable, Extensible Toolkit for Scientific Computation (PETSc), a software suite built for solving systems of PDEs in physics contexts. Among other things, PETSc is also used to simulate geodynamic processes [44] and, more relevantly, binary black hole systems [45].

The holographic bulk equations we need to solve are some of the hardest general relativity problems ever numerically computed, and they require a supercomputer. We started off with Leiden's ALICE supercomputer, but we eventually moved to Snellius, the Dutch national supercomputer which opened in September 2021.

The HoloCode works as follows. It requires the values of the normalised temperature $T/\mu$, lattice amplitude $A/\mu$ and lattice wavevector $G/\mu$ as

*We will refer to the equilibrium value of the chemical potential, $\mu_0$, as simply $\mu$, for ease of notation.

input parameters[†]. Based on the last two, the stress-energy tensor in the bulk will be constructed using the GKPW rule, and the Einstein equations will be solved using an ansatz in such a way that the solution is a black hole metric with the correct Hawking temperature. We call such a solution for certain values of $T/\mu$, $A/\mu$ and $G/\mu$ a "background".

This background, however, is an immensely long expression, taking up several megabytes of data. Therefore, the extraction of the transport and thermodynamic properties of the holographic metals using the GKPW rule also needs to be done numerically, although we do not necessarily need the supercomputer to do this. The thermodynamic properties follow directly from the GKPW rule, but for the conductivities we need to put in a but more work: we must perturb the bulk metric to induce a small electric field and thermal gradient in the boundary, and then calculate the resulting electric and heat currents. This is a rather technical process that is covered for the RN metal in [46]. We then collect the properties calculated from backgrounds of various $T/\mu$, $A/\mu$ and $G/\mu$ into a single table, which we can then use to plot the properties of the metal.

Much research has already been done into the Reissner-Nördstrom metal this way, and much of it is covered in the theses of Martijn Janse [32] and Sam Arend [33]: an external magnetic field was even implemented in the HoloCode in the RN case. However, the Gubser-Rocha metal was only implemented into the HoloCode in the second half of last year, since its more complex bulk makes the numerical computations much harder than for the RN metal. The brand new GR results will thus be the highlight of this thesis, although we will always include the corresponding RN results as a comparison.

## 4.2 Drude theory

Using the the data we will acquire using the previously described methods, we would like to find a theoretical framework that can make sense of it. Luckily, the properties of holographic metals suggest a certain model, one that might seem rather unlikely at first: Drude theory. We have finally come back to what we hinted at in the introduction of this thesis: Drude theory is much more widely applicable than only to systems of classical particles, which was the reason for its initial success. In this section, we will discuss four variations of relativistic Drude theory, and how to check them using our HoloCode data.

[†] $\mu_0$ cannot be chosen independently from the temperature in the HoloCode.

### 4.2.1 Basic Drude

In its simplest version, it works as such. Let us assume that momentum is the only long-lived quantity in our metal relative to other quantities, or in other words, that the momentum relaxation time is far larger that all other relaxation times in the system. For holographic metals, this does not seem to be too unreasonable: momentum will be relatively long-lived because it would be conserved if not for the ionic lattice, and all non-conserved quantities have relaxation times of the order of the only other timescale in the problem, the extremely small Planckian radius of the Euclidean time circle $\hbar/(k_B T)$.

Using only this assumption, it turns out that we can use the so-called Memory Matrix Formalism to find that the optical conductivity $\sigma(\omega)$ is given by [41, 47]:

$$\sigma(\omega) = \frac{\rho^2}{\mathcal{E}+\mathcal{P}} \frac{1}{(\Gamma_L - i\omega)} \tag{4.2}$$

Here, $\rho$, $\mathcal{E}$ and $\mathcal{P}$ are the charge, energy and pressure densities of the metal, respectively, and $\Gamma_L = 1/\tau_L$ is called the longitudinal momentum relaxation rate. But this is just the relativistic generalisation of Eq. 1.3, where we replace $ne \to \rho$ and $nm \to \mathcal{E}+\mathcal{P}$ to go to the relativistic regime. In the same way, expressions for $\alpha(\omega)$ and $\bar{\kappa}(\omega)$, the other conductivities in the thermoelectric conductivity matrix (Eq. 1.1), can be derived [41][‡]:

$$\begin{aligned} \alpha(\omega) &= \frac{\rho s}{\mathcal{E}+\mathcal{P}} \frac{1}{(\Gamma_L - i\omega)} \\ \bar{\kappa}(\omega) &= \frac{s^2 T}{\mathcal{E}+\mathcal{P}} \frac{1}{(\Gamma_L - i\omega)} \end{aligned} \tag{4.3}$$

Here, $s$ is the entropy density. Now, using our HoloCode, we can calculate the conductivities and all thermodynamic quantities in the DC limit ($\omega = 0$): the only thing we cannot directly derive is $\Gamma_L$. However, we can still check if the above model is correct by calculating $\Gamma_L$ from each conductivity and comparing them: we will show our results in the next chapter.

### 4.2.2 Incoherent Drude: model A

The model given in the previous section is not just basic, it might be a bit too basic. The problem is that its derivation relies on the fact that the electric

[‡] $\bar{\alpha} = \alpha$ in time-reversal symmetric systems due to the Onsager reciprocal relations [48].

and heat currents are coupled. This is not a strange assumption: charged particles carry heat, so if you move charge, you will also move heat. But this argument fails for processes that are charge conjugation symmetric: or in other words, there is as much positive charge in the system as negative charge. After all, in this case, an electric current will move charge but no heat, as an equal number of particles will move in opposite directions.

Such charge conjugation symmetric processes do not occur in classical electron systems, but in our locally quantum critical metals, it turns out there are. Studying the hydrodynamic properties of the electrons in the metal, it turns out extra terms are possible in Eqs. 4.2 and 4.3, given by [9, 41]:

$$\begin{aligned} \sigma &= \frac{\rho^2}{\mathcal{E}+\mathcal{P}}\frac{1}{(\Gamma_L - i\omega)} + \sigma_Q(\omega) \\ \alpha &= \frac{\rho s}{\mathcal{E}+\mathcal{P}}\frac{1}{(\Gamma_L - i\omega)} - \frac{\mu}{T}\sigma_Q(\omega) \\ \bar{\kappa} &= \frac{s^2 T}{\mathcal{E}+\mathcal{P}}\frac{1}{(\Gamma_L - i\omega)} + \frac{\mu^2}{T}\sigma_Q(\omega) \end{aligned} \tag{4.4}$$

Here $\sigma_Q$ is also called an incoherent conductivity, since we usually call a Drude response "coherent". Its precise physical interpretation is unclear: one possibility is that it is connected to pair production, since that is a charge conjugation symmetric process that can only happen in relativistic systems.

In the DC limit, we now have two unknown parameters, $\Gamma_L$ and $\sigma_Q$. However, we can still check the validity of this model: using two of the conductivities, we can calculate $\Gamma_L$ and $\sigma_Q$ and attempt to fit the third conductivity using Eq. 4.4. We will show our results next chapter.

### 4.2.3 Incoherent Drude: model B

The model of the last subsection is not the only way to add an incoherent conductivity to the Drude model. In fact, an alternate model appears in a system very close to the one we are studying: the 1D ionic lattice. Instead of using the 2D lattice modulation in Eq. 4.1, we modulate $\mu$ like this:

$$\mu(x,y) = \mu_0\left(1 + \frac{A}{\mu_0}\cos(Gx)\right) \tag{4.5}$$

Miraculously, a boundary with this lattice will have an exactly solvable bulk! For the RN metal, the DC conductivities are given by [49]:

$$\begin{aligned}\sigma &= \frac{1}{\int e^{B^{(0)}}} + \frac{\left(\int e^{B^{(0)}} \frac{a_t^{(0)}}{H_{tt}^{(0)}}\right)^2}{X \int e^{B^{(0)}}} \\ \alpha &= 4\pi \frac{\int e^{B^{(0)}} \frac{a_t^{(0)}}{H_{tt}^{(0)}}}{X} \\ \bar{\kappa} &= (4\pi)^2 T \frac{\int e^{B^{(0)}}}{X}\end{aligned} \tag{4.6}$$

For the GR metal, they are given by [50]:

$$\begin{aligned}\sigma &= \frac{1}{\int \frac{\gamma^{1/2}}{g_1^{1/2} Z^{(0)}}} + \frac{\left(\int \frac{\gamma^{1/2} a_t^{(0)}}{g_1^{1/2}}\right)^2}{X \int \frac{\gamma^{1/2}}{g_1^{1/2} Z^{(0)}}} \\ \alpha &= \frac{4\pi}{X} \int \frac{\gamma^{1/2} a_t^{(0)}}{g_1^{1/2}} \\ \bar{\kappa} &= \frac{(4\pi)^2 T}{X} \int \frac{\gamma^{1/2}}{g_1^{1/2} Z^{(0)}}\end{aligned} \tag{4.7}$$

$X$ and the integrals in these expressions are integrals over the holographic bulk and they have rather abstract integrands. The most important part of these expressions, however, is their form. They are of the same form as the DC limit of a Drude model where only $\sigma$ has an incoherent term:

$$\begin{aligned}\sigma(\omega) &= \frac{\rho^2}{\mathcal{E}+\mathcal{P}} \frac{1}{(\Gamma_L - i\omega)} + \sigma_{Q=0}(\omega) \\ \alpha(\omega) &= \frac{\rho s}{\mathcal{E}+\mathcal{P}} \frac{1}{(\Gamma_L - i\omega)} \\ \bar{\kappa}(\omega) &= \frac{s^2 T}{\mathcal{E}+\mathcal{P}} \frac{1}{(\Gamma_L - i\omega)}\end{aligned} \tag{4.8}$$

Here, $\sigma_{Q=0}$ is named as such because it can be derived that:

$$\sigma_{Q=0} = \sigma - \frac{\alpha^2 T}{\bar{\kappa}} \tag{4.9}$$

This is the equation for the conductivity at zero heat current. In other words, $\sigma_{Q=0}$ is a measure for how well the electric current flows if there is no heat current. This sounds similar to the pair production of model A, but these equations are clearly of a different form. One possibility could be that the finite $\sigma_{Q=0}$ signifies the presence of a neutral excitation, since then on can make an electric field and a thermal gradient conspire in such a way that only an electric current flows - but this is just speculation. This model is not only found in the 1D lattice: it is also found when translational symmetry is broken by inserting a massive scalar field in the bulk [41].

Only one conductivity now has an incoherent term, so the comparison method we use for model A will not work well here. Instead, in the DC limit, we will calculate $\sigma_{Q=0}$ from the conductivity pairs $\sigma$, $\alpha$ and $\sigma, \bar{\kappa}$ and compare the results to Eq. 4.9, and also calculate $\Gamma_L$ from one of $\alpha$ and $\bar{\kappa}$ and try to fit the other of the two conductivities with it. We will show the results next chapter. We will also test how well this Drude model matches the 1D lattice model, for which we can get data without using a supercomputer: we will show these results in the Appendix.

### 4.2.4 Incoherent Drude: model C

Not too long ago, we started suspecting in our research group that another quantity might play a large role in the transport in holographic metals:

$$\kappa = \bar{\kappa} - \frac{\alpha^2 T}{\sigma} \tag{4.10}$$

This is the thermal conductivity at zero electric current. Because of its suspected importance, we will try one other incoherent Drude model:

$$\begin{aligned} \sigma(\omega) &= \frac{\rho^2}{\mathcal{E}+\mathcal{P}} \frac{1}{(\Gamma_L - i\omega)} \\ \alpha(\omega) &= \frac{\rho s}{\mathcal{E}+\mathcal{P}} \frac{1}{(\Gamma_L - i\omega)} \\ \bar{\kappa}(\omega) &= \frac{s^2 T}{\mathcal{E}+\mathcal{P}} \frac{1}{(\Gamma_L - i\omega)} + \kappa(\omega) \end{aligned} \tag{4.11}$$

We work in the $T << \mu$ limit, and there, it is not all that surprising that $\kappa$ plays such an outsize role in transport. For the charge density $\rho$ and $\mathcal{E}+\mathcal{P}$, no meaningful temperature dependence has ever been measured for

$T << \mu$ [15]. So for the RN metal, where $S \sim T^0$, the prefactors of $1/\Gamma_L$ and $\sigma_Q$ for each of the conductivities in Eq. 4.4 are of the order:

$$\begin{aligned} \sigma &\sim T^0 \frac{1}{\Gamma_L} + T^0 \sigma_Q \\ \alpha &\sim T^0 \frac{1}{\Gamma_L} - T^{-1} \sigma_Q \\ \bar{\kappa} &\sim T^1 \frac{1}{\Gamma_L} + T^{-1} \sigma_Q \end{aligned} \tag{4.12}$$

As we can see, $\bar{\kappa}$ relatively has the largest incoherent part of all the conductivities by far for $T << \mu$. For the GR metal, the differences in scale between the incoherent parts become even larger as the Drude parts of $\alpha$ and $\bar{\kappa}$ are further suppressed by the Sommerfeld entropy.

Besides all this, we have no idea what Eq. 4.11 would signify physically, nor is it based on anything, but we might as well check it in a similar way to what we will do for model B. In the DC limit, we will calculate $\kappa$ from the conductivity pairs $\sigma$, $\bar{\kappa}$ and $\alpha$, $\bar{\kappa}$ and compare the results to Eq. 4.10, and also calculate $\Gamma_L$ from one of $\sigma$ and $\alpha$ and try to fit the other of the two conductivities with it. We will show the results next chapter.

## 4.3 The hydrodynamic regime and the linear resistivity

Now that we know about the momentum dissipation rate $\Gamma_L$ and its relationship with the electric conductivity $\sigma$, we can finally discuss the significance of the wavevector $G$ of the ionic potential. As we discussed before, both the RN and GR metals are locally quantum critical, meaning that they are divided in uncorrelated patches of highly correlated quantum critical matter. When we now introduce the ionic lattice, we find the qualitative properties of the metal depend greatly on whether $G << \mu$ or $G >> \mu$.

The latter regime is called the generalised Lindhard continuum, named after the Lindhard continuum found in Fermi liquids. In this regime, the potential influences the long ranged entangled matter within each patch, and $\Gamma_L$ and thus the resistivity $\rho$[§] scale as $\Gamma_L \sim \rho \sim T^{2\nu-1}$ [47, 51]. For the GR metal,

[§]In the regime we work in, $T << \mu$, no significant temperature dependence of the charge density (!) $\rho$ or $\mathcal{E} + \mathcal{P}$ has ever been observed [15].

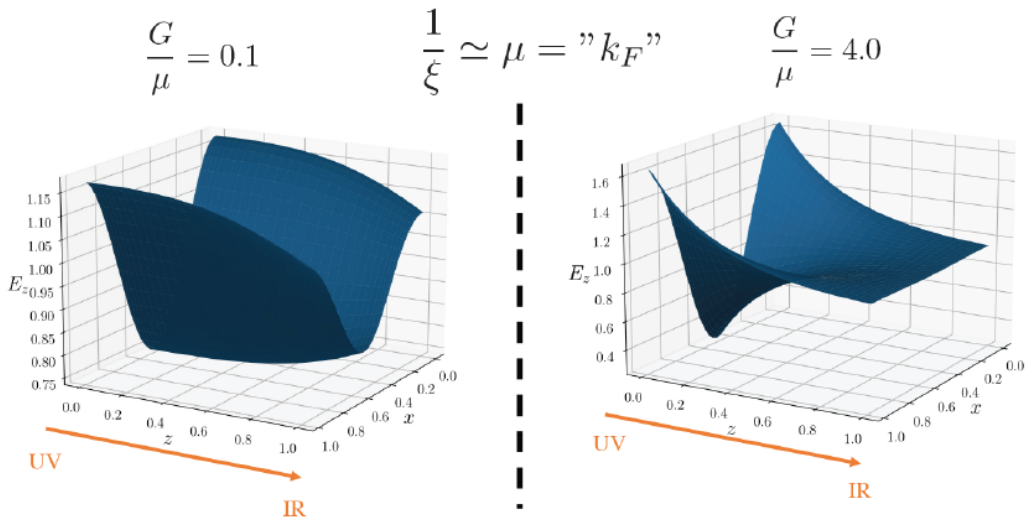


***Figure 4.1:*** *Plot of a single period of the electrostatic potential $A_t$ in the bulk at different values of $z = 1/r$ in both the hydrodynamical regime (left) and the generalised Lindhard continuum (right) [32]. $z = 0$ marks the boundary (i.e. the UV), and we go deeper into the IR as $z$ increases.*

we may interpret this as the generalised version of the $\rho \sim T^2$ scaling in Fermi liquids, with an anomalous dimension $\nu$ that depends on $G$.

However, things get more interesting in the regime where $G << \mu$. This is the hydrodynamical regime, where the potential is approximately constant within a single patch and therefore only influences the collective hydrodynamics of the different patches. This has two surprising consequences. Firstly, as shown by Martijn Janse for the RN metal in his thesis [32] (see Fig. 4.1), there is a qualitative difference in how the ionic potential influences macroscopic properties in the hydrodynamical and generalised Lindhard regimes. In the latter, the corresponding modulation of the electrostatic potential $A_t$ in the bulk essentially vanishes in the IR, meaning it only meaningfully influences the macroscopic properties of the system by influencing the values of its parameters.

However, in the hydrodynamical regime, the story is very different. Here, the modulation stays significant for much longer as we go to the IR, meaning the ionic potential has a macroscopic prescence in the metal! As an analogy, it is as if the electron fluid in the metal streams past a periodic formation of pebbles.

Now, the second consequence is the most important one. As the electron fluid

streams through the pebbles of the ionic potential, its resulting momentum relaxation must in a large part be governed by the viscosity $\eta$ of the fluid: we expect momentum to relax more quickly if the fluid is more viscous. In fact, by using dimensional analysis we can find that $\Gamma_L \sim \eta$ [15, 52]. Furthermore, according to the dictionary, the viscosity corresponds to the zero frequency absorption cross section of gravitational waves by the black hole in the bulk [15], which is just proportional to the black hole are $A$. Taking all this and earlier results together, we can find:

$$\rho \sim \Gamma_L \sim \eta \sim A \sim S \tag{4.13}$$

So, in the GR metal, the Sommerfeld entropy now gives us the elusive linear-in-$T$ resistivity! As Jonah Post shows in his thesis, both $S \sim T$ and $\rho \sim T$ are clearly seen in the data, confirming this prediction. There is a much deeper physics story here, particularly revolving around the viscosity, but Jonah already explains that very well: what is important to this thesis is that real life cuprates live in the hydrodynamical regime, and thus all our data be in this regime, with $G$ never higher than $\mu$.

Chapter 5

# Results

Now, we will present our results of checking the four Drude models in the previous chapter.

## 5.1 Basic Drude

As can be seen from Fig. 5.1 and especially Fig. 5.2, the $\Gamma_L$ calculated from $\sigma$, $\alpha$ and $\bar{\kappa}$ using the basic Drude model match quite well at low $A/\mu$ but diverge significantly at high $A/\mu$, for both the RN and the GR metal. As we expected, the basic Drude model is too simple to describe the high $A/\mu$ cuprates. However, at low $T$, the GR $\Gamma_L$ all scale as $\Gamma_L \sim T$, which, along with the good matching at low $A/\mu$, is a good sign that we are on the right track.

## 5.2 Incoherent Drude: model A

As can be seen in Fig 5.3, the calculated $\Gamma_L$ do not look much better than before at first glance: $\Gamma_{L,\sigma,\bar{\kappa}}$ and $\Gamma_{L,\sigma,\alpha}$ match somewhat well, but $\Gamma_{L,\alpha,\bar{\kappa}}$ is way off compared to the other two. The discrepancies are even larger in $\sigma_Q$, as shown in Fig. 5.4: not even its sign or if it increases or decreases in $A$ are consistent. It's notable, however, that $\sigma_Q$ is always much smaller than $1/\Gamma_L$. This suggests any incoherent terms are much smaller than the Drude terms, which explains why basic Drude matches so well for low $A$, since $\Gamma_L \to \infty$ as $A \to 0$.

With all this in mind, Figs. 5.5 and 5.6 show a rather unexpected outcome

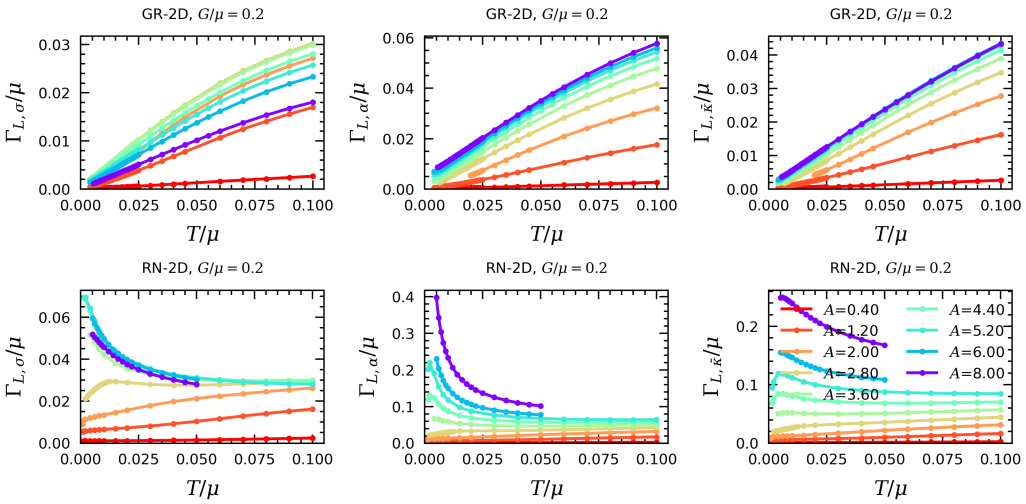


***Figure 5.1:*** *Plots of $\Gamma_L/\mu$ as calculated from the three conductivities $\sigma$, $\alpha$ and $\bar{\kappa}$ (denoted by the subscripts of $\Gamma_L$) using the basic Drude model, at $G/\mu = 0.2$ as a function of $T/\mu$ for various values of $A/\mu$. The top plots are for the 2D GR metal, the bottom plots for the 2D RN metal.*

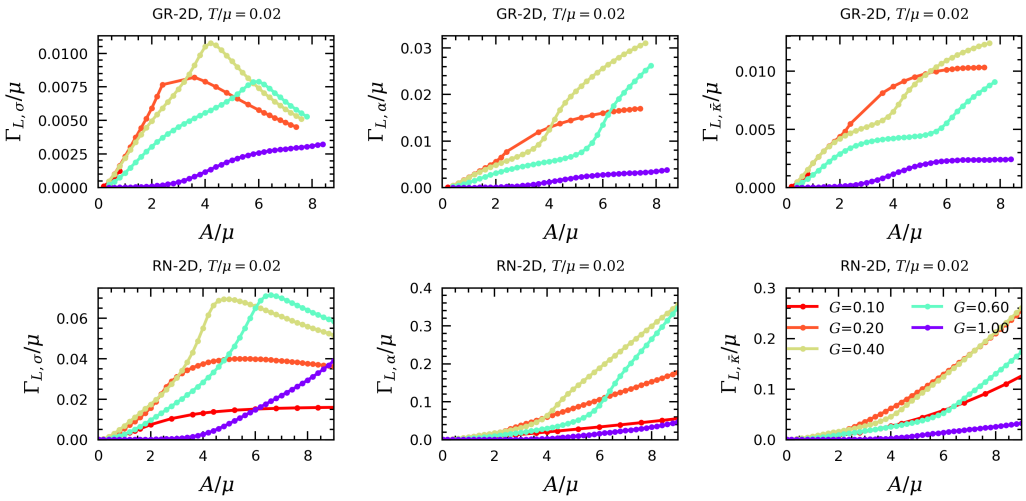


***Figure 5.2:*** *Plots of $\Gamma_L/\mu$ as calculated from the three conductivities $\sigma$, $\alpha$ and $\bar{\kappa}$ (denoted by the subscripts of $\Gamma_L$) using the basic Drude model, $T/\mu = 0.02$ as a function of $A/\mu$ for various values of $G/\mu$. The top plots are for the 2D GR metal, the bottom plots for the 2D RN metal.*

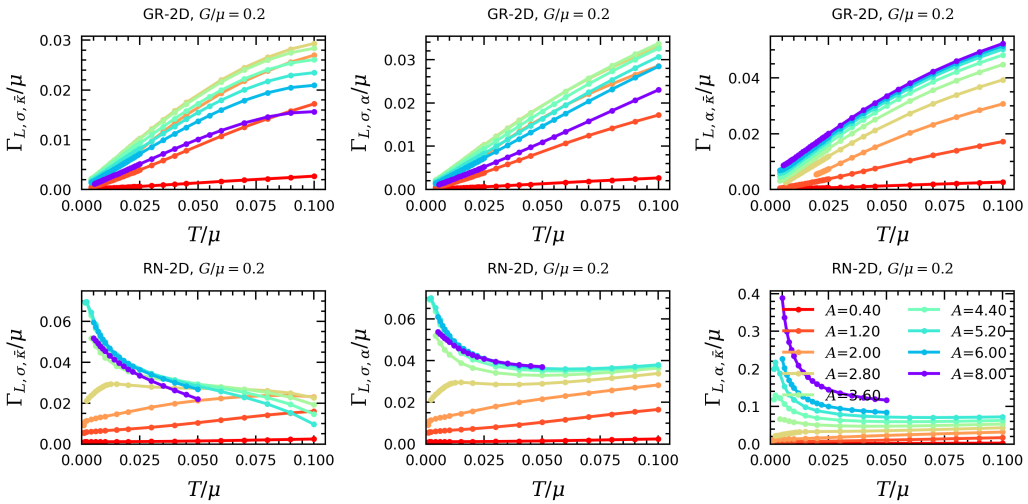


***Figure 5.3:*** *Plots of $\Gamma_L/\mu$ as calculated from each pair among the three conductivities $\sigma$, $\alpha$ and $\bar{\kappa}$ (denoted by the subscripts of $\Gamma_L$) using incoherent Drude model A, at $G/\mu = 0.2$ as a function of $T/\mu$ for various values of $A/\mu$. The top plots are for the 2D GR metal, the bottom plots for the 2D RN metal.*

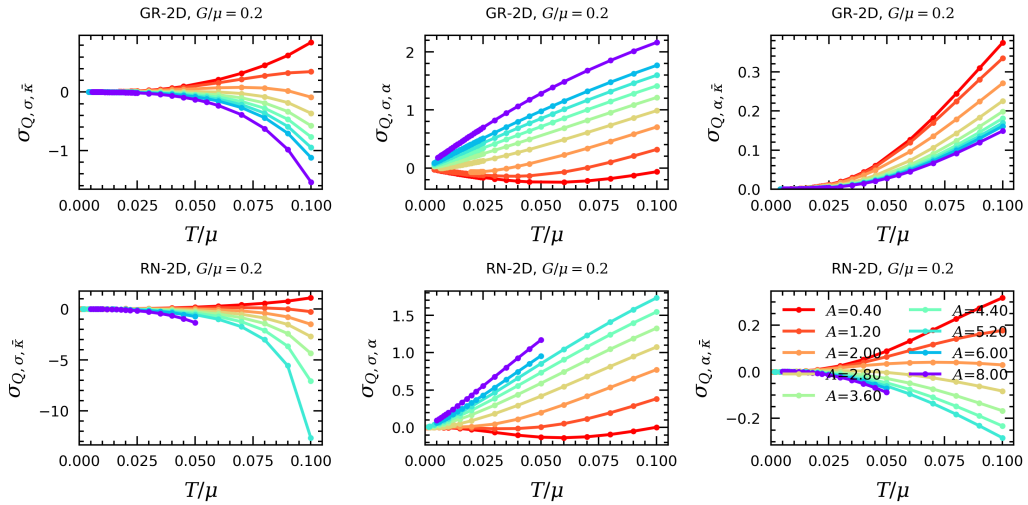


***Figure 5.4:*** *Plots of $\sigma_Q$ as calculated from each pair among the three conductivities $\sigma$, $\alpha$ and $\bar{\kappa}$ (denoted by the subscripts of $\sigma_Q$) using incoherent Drude model A, at $G/\mu = 0.2$ as a function of $T/\mu$ for various values of $A/\mu$. The top plots are for the 2D GR metal, the bottom plots for the 2D RN metal.*

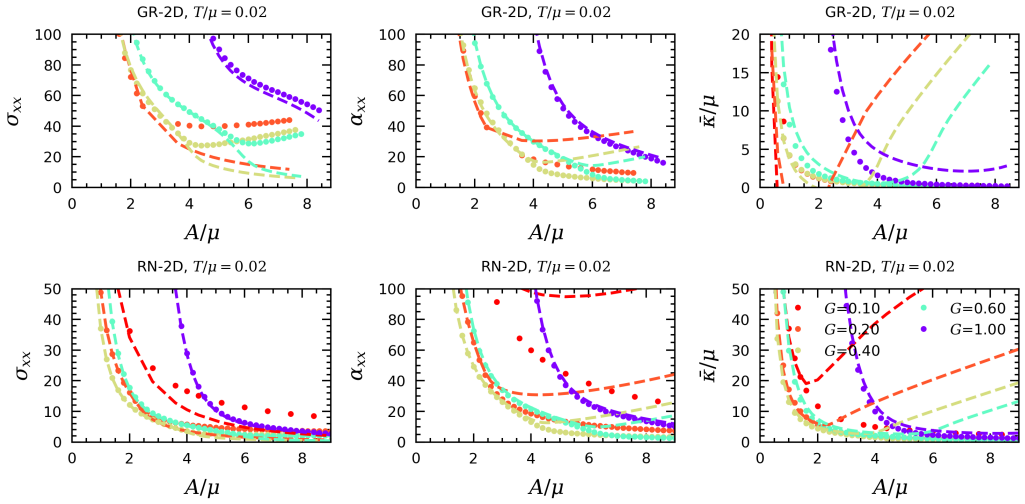


***Figure 5.5:*** *Fits of each of the three conductivities $\sigma$, $\alpha$ and $\bar{\kappa}$ calculated from the other two conductivities using incoherent Drude model A, plotted at $T/\mu = 0.02$ as a function of $A/\mu$ for various values of $G/\mu$. The top plots are for the 2D GR metal, the bottom plots for the 2D RN metal. The dots denote the actual conductivities, the dashed lines are the fits.*

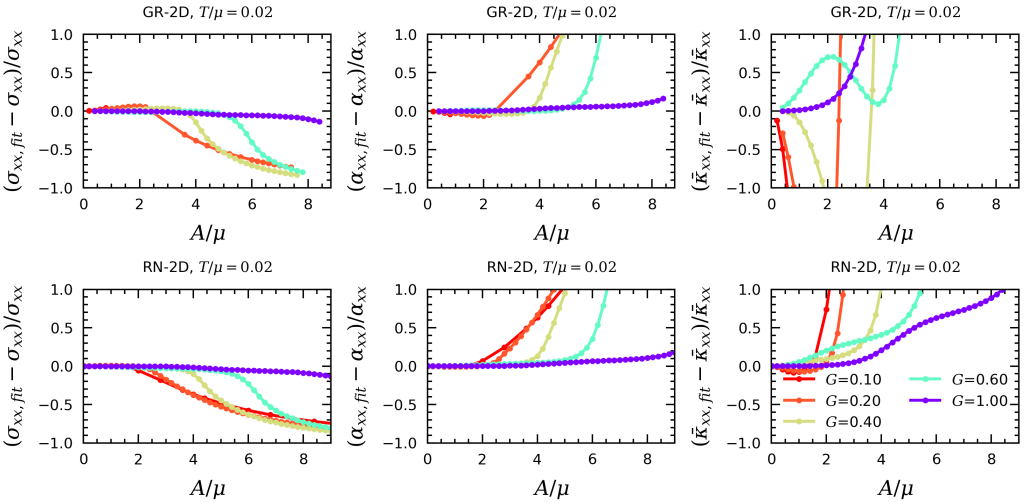


***Figure 5.6:*** *The relative differences of each of the conductivity fits in Fig. 5.5 with their respective conductivities. The top plots are for the 2D GR metal, the bottom plots for the 2D RN metal.*

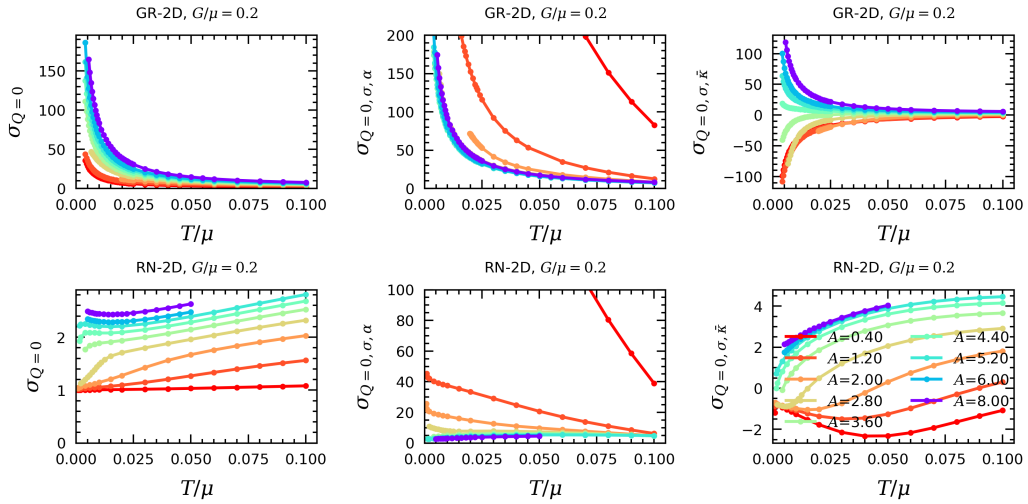


***Figure 5.7:*** *$\sigma_{Q=0}$ as calculated, from left to right, by using Eq. 4.9 and by using incoherent Drude model B via the conductivity pairs $\sigma$, $\alpha$ and $\sigma$, $\bar{\kappa}$, plotted at $G/\mu = 0.2$ as a function of $T/\mu$ for various values of $A/\mu$. The top plots are for the 2D GR metal, the bottom plots for the 2D RN metal.*

for the conductivity fits: the fits of $\sigma$ and $\alpha$ match incredibly well for both the GR and RN metals up to a certain value of $A/\mu$ that increases with $G/\mu$, after which the fit rapidly diverges. $\bar{\kappa}$ is the outlier, especially in the GR metal, but this might be a consequence of the large influence of $\sigma_Q$ on $\bar{\kappa}$: small deviations in the fits of $\sigma$ and $\alpha$ seem to blow up for $\bar{\kappa}$. So the odd behaviour of $\bar{\kappa}$ might simply be an issue of numerics, although it is still very uncertain.

## 5.3 Incoherent Drude: model B

Just like the fits of $\sigma_Q$ in model A, the fits for $\sigma_{Q=0}$ are all over the place, especially for the RN metal, as can be seen from Fig. 5.7. However, if we look a bit closer, we can see that the lines of the different plots seem to saturate onto the same curve at high $A$: this could signify a match!

Furthermore, something interesting happens in Figs. 5.8 and 5.9: the fits start deviating much sooner than in model A, but at the values of $A/\mu$ where that model starts to deviate, the deviation flattens out as a function of $A/\mu$, or in the case of the RN metal, it might even bend back to 0. This lends support to the idea that the high $A/\mu$ behaviour of the metals is well described by model B. Lastly, it seems the values of $A/\mu$ where the model A

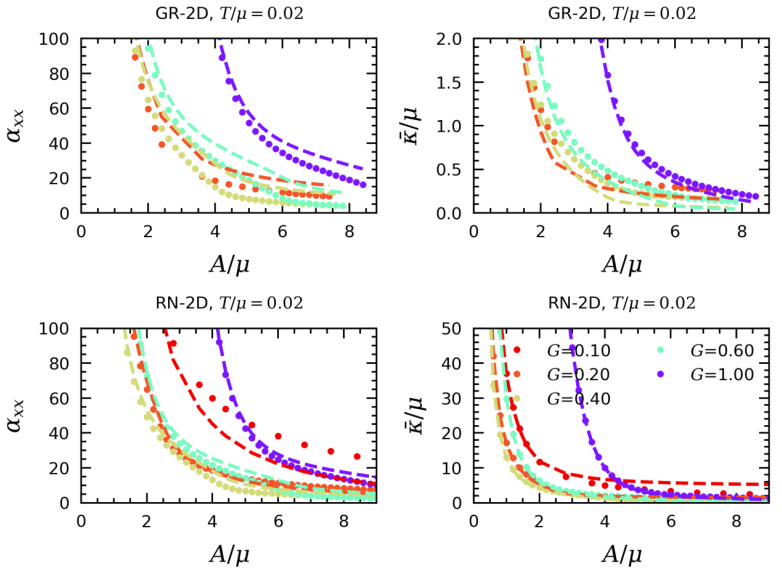


***Figure 5.8:*** *Fits of the two conductivities $\alpha$ and $\bar{\kappa}$ using the value of $\Gamma_L$ calculated from the other conductivity with incoherent Drude model B, plotted at $T/\mu = 0.02$ as a function of $A/\mu$ for various values of $G/\mu$. The top plots are for the 2D GR metal, the bottom plots for the 2D RN metal. The dots denote the actual conductivities, the dashed lines are the fits.*

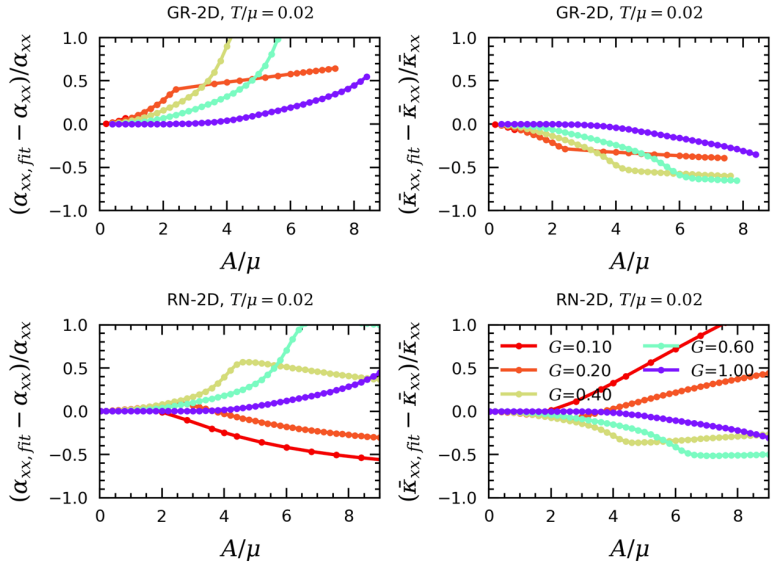


***Figure 5.9:*** *The relative differences of each of the conductivity fits in Fig. 5.8 with their respective conductivities. The top plots are for the 2D GR metal, the bottom plots for the 2D RN metal.*

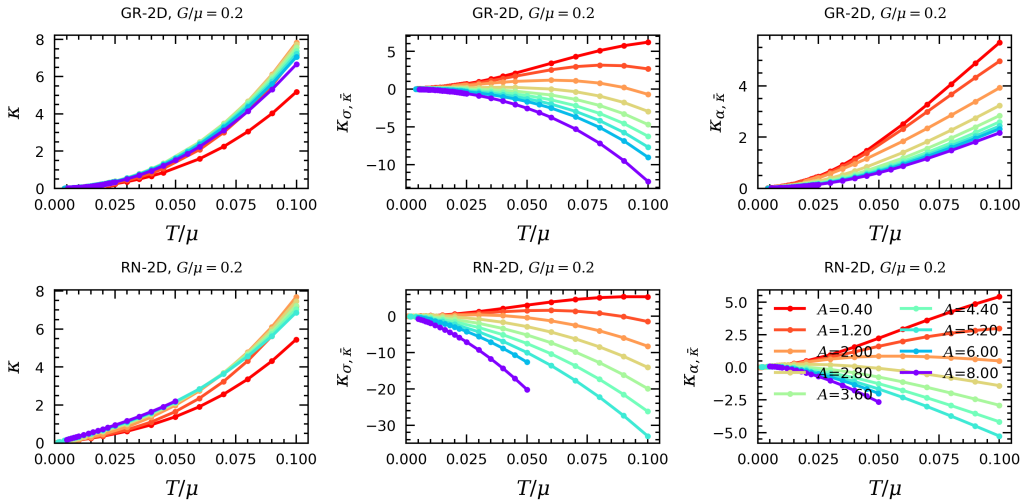


***Figure 5.10:*** *$\kappa$ as calculated, from left to right, by using Eq. 4.10 and by using incoherent Drude model C via the conductivity pairs $\sigma$, $\bar{\kappa}$ and $\alpha$, $\bar{\kappa}$, plotted at $G/\mu = 0.2$ as a function of $T/\mu$ for various values of $A/\mu$. The top plots are for the 2D GR metal, the bottom plots for the 2D RN metal.*

fits deviate and the model B fits inflect are special in some way, and we will discuss them more in the next chapter.

## 5.4 Incoherent Drude: model C

In Fig. 5.10, we now see the opposite of what we saw for $\sigma_{Q=0}$ in model B: $\kappa$ seems all over the place, but the different plots all saturate onto roughly the same curve for low $A/\mu$, so we might have a match at low $A/\mu$ now! Meanwhile, Figs. 5.11 and 5.12 strongly resemble our results in model A: the fits match at low $A/\mu$ and then suddenly deviate at the same values of $A/\mu$ as before. This could once again simply be due to the large relative size of the incoherent part of $\bar{\kappa}$: the other incoherent parts are negligible by comparison.

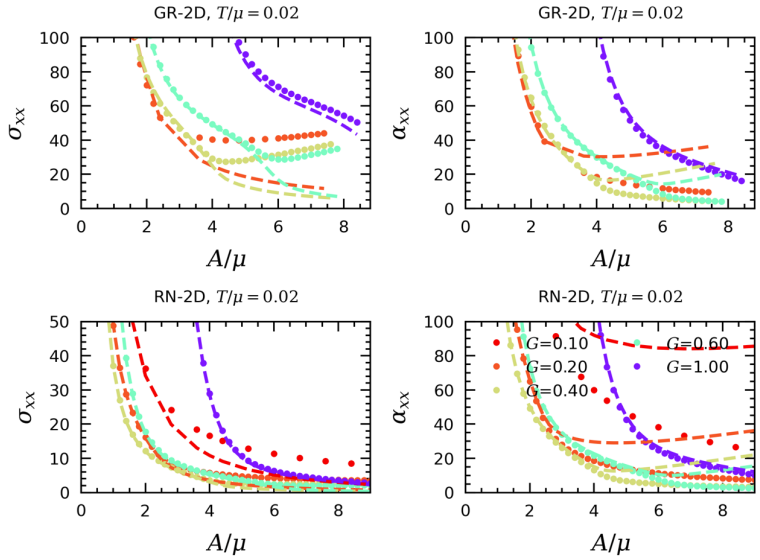


***Figure 5.11:*** *Fits of the two conductivities $\sigma$ and $\alpha$ using the value of $\Gamma_L$ calculated from the other conductivity with incoherent Drude model C, plotted at $T/\mu = 0.02$ as a function of $A/\mu$ for various values of $G/\mu$. The top plots are for the 2D GR metal, the bottom plots for the 2D RN metal. The dots denote the actual conductivities, the dashed lines are the fits.*

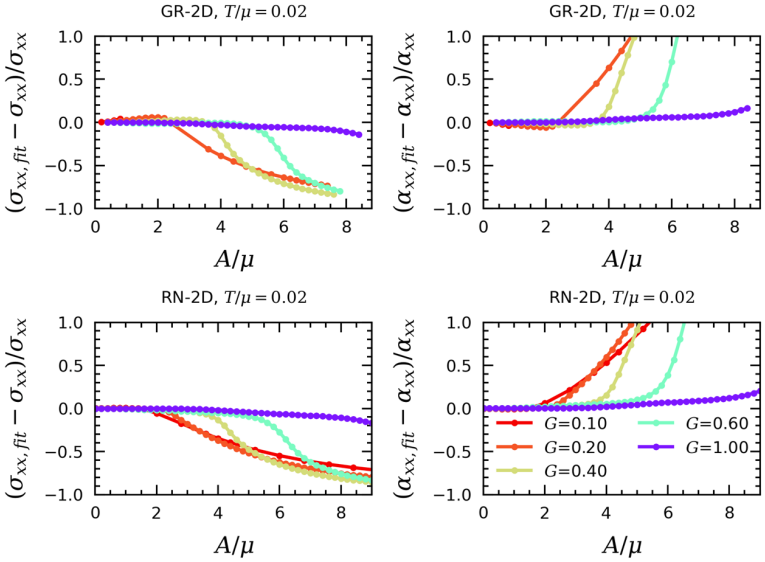


***Figure 5.12:*** *The relative differences of each of the conductivity fits in Fig. 5.11 with their respective conductivities. The top plots are for the 2D GR metal, the bottom plots for the 2D RN metal.*

Chapter 6

# Discussion

Using the conductivities and thermodynamic quantities calculated using the HoloCode for both the RN and GR metals, we have tested the consistency of four different Drude models: the most basic relativistic Drude model, and three models with different incoherent terms, named model A, B and C.

The results are somewhat surprising. Model A, usually the most conventional model with incoherent conductivities, fails for all values of $A$: the only reason that the fits of the conductivities still look right for low A is that the incoherent parts of $\sigma$ and $\alpha$ are relatively much smaller than the incoherent part of $\bar{\kappa}$ for $T << \mu$. Models B and C are much more successful: the former matches well with the data for large $A$, while the latter matches well for low $A$. The crossover values of $A/\mu$ between these two regimes of validity depend on $G/\mu$, and they are also visible in the 1D lattice RN and GR metals, as seen in the Appendix.

The fact that there seem to be two different regimes that obey two different Drude models is quite puzzling. Drude theory normally does not allow for something like this to happen, so how is this possible? In our research group, we already have a possible answer available. Recent calculations of the optical conductivity of the GR metal at finite $A$, seem to indicate $\sigma(\omega)$ does not obey Drude theory at all, but its coherent part is instead given by:

$$\sigma_{coh.}(\omega) = \frac{\rho^2}{\mathcal{E}+\mathcal{P}} \frac{\Omega - i\omega}{(\Gamma_L - i\omega)(\Omega - i\omega) + \omega_0^2} \tag{6.1}$$

The reason that the DC conductivities still look so Drude-like is that Eq. 6.1

reduces to a Drude form at $\omega = 0$, with an effective momentum relaxation rate equal to $\Gamma_{L,eff.} = \Gamma_L + \omega_0^2/\Omega$.

To see why all this is significant, we must look at the poles of the conductivities. A pole is a divergence of $\sigma(\omega)$, where it becomes infinite. Since the conductivity is a response function of the system, poles are thus located at values of $\omega$ which the system very strongly responds to, which means the locations of poles give very useful information about the intrinsic properties of the system.

Poles do not have to be on the real $\omega$-axis, they can be anywhere on the complex plane: poles on the real axis are called normal modes, which indicate a resonance of the system; poles on the imaginary axis are called relaxational modes, which indicate a relaxation of the system; and off-axis poles are quasi-normal modes, resonances that decay over time. For example, Drude theory only has one pole, a relaxational pole at $\omega = -i\Gamma_L$, signifying momentum is the only long-lived quantity in the system that is relevant to transport.

However, the story is more interesting for Eq. 6.1. The poles of this equation are:

$$\omega_\pm = -\frac{i}{2}(\Gamma_L + \Omega) \pm \frac{i}{2}\sqrt{(\Gamma_L - \Omega)^2 - 4\omega_0^2} \tag{6.2}$$

Assuming $\Omega > \Gamma_L$, the momentum relaxation pole is located at $\omega_-$, since it reduces to $\omega_- = -i\Gamma_L$ at $\omega_0 = 0$. We believe $\omega_+$ is then connected to charge diffusion, but that inquiry is still in progress. The important part, however, is that if $\omega_0$ increases past $|\Gamma_L - \Omega|/4$, these two relaxational poles will collide and split up into two quasi-normal modes! Such pole collisions can dramatically alter the properties of the system, even in the DC limit. In this case, the momentum relaxation pole is no longer present in the conventional sense, causing hydrodynamics to break down, as also seen in other holographic systems [53].

The main point is that it might not be unthinkable that this (or another) pole collision is causing the transition from low-$A$ $\kappa$-dominated transport to high-$A$ $\sigma_{Q=0}$-dominated transport. More research into the optical transport of the GR (and maybe RN) metals needs to be done to verify this theory, though, and this is beyond the scope of this thesis. Joost Aretz covers the optical conductivity of the homogeneous ($A = 0$) GR metal in his thesis, however, and also investigates the poles in that system [54].

Our results have a few more caveats. Firstly, as of right now, we have no sure

physical interpretation of what a system that obeys model B or C incoherent Drude transport would look like, nor do we know why the transition between the models happens at the values of $A/\mu$ and $G/\mu$ that it does: this will require more thinking. Secondly, in model B, the fits of $\sigma_{Q=0}$ match well at high $A$, but the conductivity fits match less well, even if their deviations inflect somewhat back to 0. We still need to figure out why this is the case.

Chapter 7

# Conclusion and outlook

## 7.1 Conclusion

We have numerically calculated the conductivities and thermodynamic quantities of the holographic Reissner-Nordström and Gubser-Rocha metals subject to an ionic potential. We have done this by running code, which our group has designed to solve the complicated Einstein equations in the bulk, on a supercomputer.

We then tested the consistency of four different Drude models for the three conductivities $\sigma$, $\alpha$ and $\bar{\kappa}$: the most basic relativistic Drude model, and three models with different incoherent terms, named model A, B and C. The result is that the most commonly used model in holography, model A, matches the data quite poorly, while model B matches quite well for large values of the lattice amplitude $A$ and model C matches well for low values of $A$: the crossover point depends strongly on the lattice wavevector $G$.

We believe the transition from $\kappa$-dominated transport (model C) to $\sigma_{Q=0}$-dominated transport (model B) is caused by a pole collision, but this needs to be further investigated by studying the optical transport of the RN and GR metals. The physical meaning of the two Drude models also needs to be investigated.

In short, the RN and GR metals are not truly governed by Drude theory, since pole collisions do not occur in Drude theory: Drude theory fails because there is another long-lived quantity besides the momentum. However, the DC transport does resemble Drude transport, although its exact form depends on which of two regimes the metal is in.

## 7.2 Outlook

Here, we will discuss possible future avenues of research into holographic metals.

### Optical transport

In this thesis, we focused on DC transport, but it is also possible to investigate the optical electric conductivity in holographic metals. This is done by using an electric field perturbation of the form $\vec{E}(x) = Ee^{-i\omega t}$ and then finding the conductivity in the same way as described in [46]. One can even break translational symmetry in an analytically tractable way in a similar manner, by adding a spatial dependence $\vec{E}(x) = \vec{E}e^{-i\omega t + i\vec{k}\cdot\vec{x}}$.

As stated before, Joost Aretz has done a lot of work on the optical transport in the Gubser-Rocha metal without an ionic lattice [54], but research on the optical transport with an ionic lattice is also underway in our group, and it is delivering promising results, as we discussed in the previous chapter. Nevertheless, there is still much work to be done.

### Magnetotransport

Aside from subjecting holographic metals to an electric field and studying their response, we can also subject them to an external magnetic field. The transport properties of the metal then immediately become a lot more interesting: the electrical conductivity matrix gains off-diagonal Hall entries $\sigma_{xy} = -\sigma_{yx}$, and the electrical conductivities will be given by:

$$\sigma_{xx}(\omega) = \frac{\rho^2}{\mathcal{E}+\mathcal{P}} \frac{1}{(\Gamma_L - i\omega)\left(1 + \frac{\omega_c^2}{\Gamma_T - i\omega}\right)^2} \tag{7.1}$$

$$\sigma_{xy}(\omega) = \sigma_{xx}(\omega)\frac{\omega_c}{\Gamma_T - i\omega} \tag{7.2}$$

Here, $\Gamma_T$ is the transversal momentum relaxation rate, and $\omega_c = \frac{\rho B}{\mathcal{E}+\mathcal{P}}$ is the cyclotron frequency, where $B$ is the magnetic field strength. $\omega_c$ marks a normal mode in the metal, making its transport properties much richer.

An external magnetic field on the boundary can be implemented in the bulk by including magnetic charge, creating a so-called dyonic black hole in the IR [55]. Martijn Janse [32] and Sam Arend [33] have already extensively

studied the magnetotransport of the RN metal, and have for example discovered that $\Gamma_L$ and $\Gamma_T$ are not necessarily the same. Since recently, it is also possible to calculate the optical conductivity of the homogeneous RN metal under a magnetic field. However, numerical code to calculate the effect of a magnetic field on the GR metal is not yet available, so there is still a whole lot to discover.

## Superconductivity

We will end this thesis with the subject where it all started: high-$T_c$ superconductivity. Much work has already been done on this subject [9, 56], and the secret behind the high critical temperature has already been discovered: superconductivity in a cuprate is subject to a generalised, quantum critical version of BCS theory, with a superconducting order parameter that is relevant under renormalisation instead of marginal like in the Fermi liquid. This means the superconducting order parameter plays a much more important role in the macroscopic properties in cuprates than it does in Fermi liquids, making it easier for the metal to become superconducting, hence the higher critical temperature.

Now we just have to find a way to create a holographic bulk that corresponds to a boundary metal that can become superconducting. The secret seems to be in the fact that the no-hair theorem of black holes does not apply in AdS space, allowing us to grant all kinds of spiky protrusions to the IR black hole [9]. The order of these protrusions translates to different orders in the boundary, allowing for phase transitions. Numerically solving the amazingly complicated bulks created by the ”hair” (they are even more complicated than the GR bulks) seems like a distant dream for now. But when we do, maybe the holy grail of condensed matter physics, a room temperature superconductor at atmospheric pressure, and the resulting potential revolution in physics, might inch just a little bit closer...

Appendix A

# Drude theory in the 1D ionic lattice

An easy way to check the validity of model B is by calculating the ratio of $\alpha$ and $\rho\bar{\kappa}/(sT)$, since that should be equal to 1. As we can see in Fig. A.1, this is true for $A \to 0$, but it fails for finite $A$. This shows the analogy between model B and the exact expressions for the conductivities is not exact, and that they are merely of the same form: the thermodynamic quantities are not equal to their analogous integral expressions in the exact equations. Nevertheless, we try to match model B to the 2D ionic lattice holographic metals in the main part of the thesis.

Interestingly, the ratios in Fig. A.1 suddenly flatten out at the same values of $A/\mu$ where we see something similar happen in the 2D lattice metals in the main part of the thesis. This could lend credence to the theory posed in the Discussion.

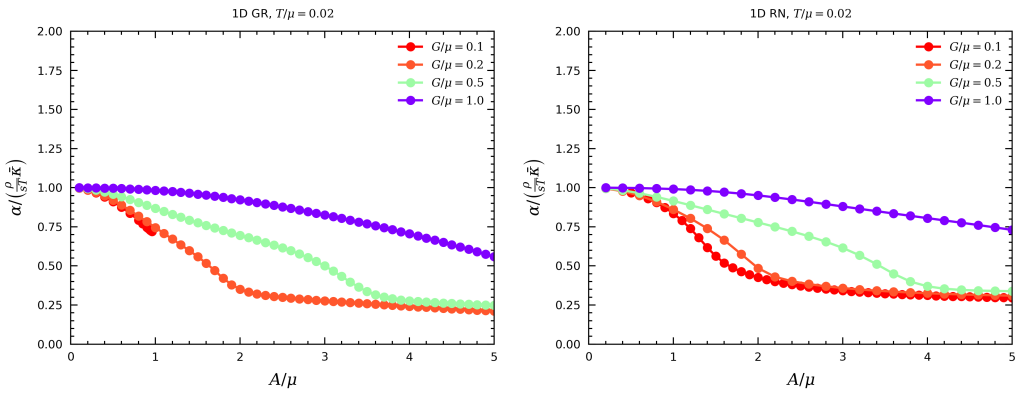


***Figure A.1:*** *Ratio of $\alpha$ and $\rho\bar{\kappa}/(sT)$ at $T/\mu = 0.02$ as a function of $A/\mu$ at various values of $G/\mu$. The GR metal is on the left, the RN metal on the right.*

# Bibliography


[1] S. A. Hartnoll, A. Lucas, and S. Sachdev, *Holographic Quantum Matter*, The MIT Press, 2018.

[2] P. Drude, *Zur Elektronentheorie der Metalle*, Annalen der Physik **306**, 566 (1900).

[3] A. Sommerfeld, *Zur Elektronentheorie der Metalle auf Grund der Fermischen Statistik*, Zeitschrift für Physik **47**, 1 (1928).

[4] J. Zaanen, *The Classical Condensates: from Crystals to Fermi-liquids*, Lorentz Institute for Theoretical Physics, Leiden University, 1996.

[5] L. D. Landau, *On the theory of the Fermi liquid*, Journal of Experimental and Theoretical Physics **35**, 97 (1958).

[6] M. Eschrig, J. A. Sauls, H. Burkhardt, and D. Rainer, *Fermi Liquid Superconductivity*, in *High-$T_c$ Superconductors and Related Materials*, edited by S.-L. Drechsler and T. Mishonov, volume 86 of *NATO Science Partnership Subseries: 3*, Springer, 2001.

[7] J. G. Bednorz and K. A. Müller, *Possible high $T_c$ superconductivity in the Ba-La-Cu-O system*, Zeitschrift für Physik B Condensed Matter **64**, 189 (1986).

[8] M. K. Wu, J. R. Ashburn, C. J. Torng, P. H. Hor, R. L. Meng, L. Gao, Z. J. Huang, Y. Q. Wang, and C. W. Chu, *Superconductivity at 93 K in a new mixed-phase Y-Ba-Cu-O compound system at ambient pressure*, Physical Review Letters **58**, 908 (1987).

[9] J. Zaanen, *Lectures on quantum supreme matter*, arXiv:2110.00961v2, 2021.

[10] B. Keimer, S. A. Kivelson, M. R. Norman, S. Uchida, and J. Zaanen, *From quantum matter to high-temperature superconductivity in copper oxides*, Nature **518**, 179 (2015).

[11] J. Ayres, M. Berben, M. Čulo, Y.-T. Hsu, E. van Heumen, Y. Huang, J. Zaanen, T. Kondo, T. Takeuchi, J. R. Cooper, C. Putzke, S. Friedemann, A. Carrington, and N. E. Hussey, *Incoherent transport across the strange-metal regime of overdoped cuprates*, Nature **595**, 661 (2021).

[12] N. E. Hussey, K. Takenaka, and H. Takagi, *Universality of the Mott-Ioffe-Regel limit in metals*, Philosophical Magazine **84**, 2847 (2004).

[13] A. Legros, S. Benhabib, W. Tabis, F. Laliberté, M. Dion, M. Lizaire, B. Vignolle, D. Vignolles, H. Raffy, Z. Z. Li, P. Auban-Senzier, N. Doiron-Leyraud, P. Fournier, D. Colson, L. Taillefer, and C. Proust, *Universal T-linear resistivity and Planckian dissipation in overdoped cuprates*, Nature Physics **15**, 142 (2019).

[14] D. van der Marel, H. J. A. Molegraaf, J. Zaanen, Z. Nussinov, F. Carbone, A. Damascelli, H. Eisaki, M. Greven, P. H. Kes, and M. Li, *Quantum critical behaviour in a high-$T_c$ superconductor*, Nature **425**, 271 (2003).

[15] J. Zaanen, *Planckian dissipation, minimal viscosity and the transport in cuprate strange metals*, SciPost Physics **6**, 061 (2019).

[16] R. Kubo, *Statistical-Mechanical Theory of Irreversible Processes. I. General Theory and Simple Applications to Magnetic and Conduction Problems*, Journal of the Physical Society of Japan **12**, 570 (1957).

[17] P. C. Martin and J. Schwinger, *Theory of Many-Particle Systems. I*, Physical Review **115**, 1342 (1959).

[18] J. Zaanen, J.-W. Sun, Y. Liu, and K. Schalm, *Holographic Duality in Condensed Matter Physics*, Cambridge University Press, 2015.

[19] J. Zaanen, F. Krüger, J.-H. She, D. Sadri, and S. I. Mukhin, *Pacifying the Fermi-liquid: battling the devious fermion signs*, arXiv:0802.2455v1, 2008.

[20] D. M. Ceperley, *Path integrals in the theory of condensed helium*, Reviews of Modern Physics **67**, 279 (1995).

[21] M. Troyer and U.-J. Wiese, *Computational Complexity and Fundamental Limitations to Fermionic Quantum Monte Carlo Simulations*, Physical Review Letters **94**, 170201 (2005).

[22] J. Maldacena, *The Large N Limit of superconformal field theories and supergravity*, Advances in Theoretical and Mathematical Physics **2**, 231 (1998).

[23] E. Witten, *Anti de Sitter space and holography*, Advances in Theoretical and Mathematical Physics **2**, 253 (1998).

[24] H. A. Kramers and G. H. Wannier, *Statistics of the Two-Dimensional Ferromagnet. Part I*, Physical Review **60**, 252 (1941).

[25] J. McGreevy, *Holographic Duality with a View Toward Many-Body Physics*, Advances in High Energy Physics **2010** (2010).

[26] S. W. Hawking, *Black hole explosions?*, Nature **248**, 30 (1974).

[27] J. D. Bekenstein, *Black holes and the second law*, Lettere al Nuovo Cimento (1971-1985) **4**, 737 (1972).

[28] S. S. Gubser, I. R. Klebanov, and A. M. Polyakov, *Gauge theory correlators from non-critical string theory*, Physics Letters B **428**, 105 (1998).

[29] M. Baggioli, *Applied Holography: A Practical Mini-Course*, SpringerBriefs in Physics, Springer, 2019.

[30] C. M. Varma, P. B. Littlewood, S. Schmitt-Rink, E. Abrahams, and A. E. Ruckenstein, *Phenomenology of the normal state of Cu-O high-temperature superconductors*, Physical Review Letters **63**, 1996 (1989).

[31] N. Iqbal, H. Liu, and M. Mezei, *Semi-local quantum liquids*, Journal of High Energy Physics **2012**, 86 (2012).

[32] M. A. Janse, *Magnetotransport and dissipation in locally quantum critical metals subject to umklapp potentials*, Master's thesis, Leiden University, 2022.

[33] S. C. Arend, *Magneto-Transport of a Reissner-Nordström Holographic Metal*, Master's thesis, Leiden University, 2022.

[34] T. Kaluza, *Zum Unitätsproblem der Physik*, Sitzungsberichte der Königlich Preußischen Akademie der Wissenschaften , 966 (1921).

[35] O. Klein, *Quantentheorie und fünfdimensionale Relativitätstheorie*, Zeitschrift für Physik **37**, 895 (1926).

[36] B. Goutéraux and E. Kiritsis, *Generalized holographic quantum criticality at finite density*, Journal of High Energy Physics **2011**, 36 (2011).

[37] R. A. Davison, S. A. Gentle, and B. Goutéraux, *Impact of irrelevant deformations on thermodynamics and transport in holographic quantum critical states*, Physical Review D **100**, 086020 (2019).

[38] S. S. Gubser and F. D. Rocha, *Peculiar properties of a charged dilatonic black hole in $AdS_5$*, Physical Review D **81**, 046001 (2010).

[39] Y. Ling, C. Niu, J.-P. Wu, and Z.-Y. Xian, *Holographic lattice in Einstein-Maxwell-dilaton gravity*, Journal of High Energy Physics **2013**, 6 (2013).

[40] A. Romero-Bermúdez, A. Krikun, K. Schalm, and J. Zaanen, *Anomalous attenuation of plasmons in strange metals and holography*, Physical Review B **99**, 235149 (2019).

[41] R. A. Davison and B. Goutéraux, *Dissecting holographic conductivities*, Journal of High Energy Physics **2015**, 90 (2015).

[42] M. Baggioli, K.-Y. Kim, L. Li, and W.-J. Li, *Holographic axion model: A simple gravitational tool for quantum matter*, Science China: Physics, Mechanics & Astronomy **64**, 270001 (2021).

[43] J. Post, *DC Transport in Gubser-Rocha Holographic Matter*, Master's thesis, Leiden University, 2022.

[44] R. F. Katz, M. G. Knepley, B. Smith, M. Spiegelman, and E. T. Coon, *Numerical simulation of geodynamic processes with the Portable Extensible Toolkit for Scientific Computation*, Physics of the Earth and Planetary Interiors **163**, 52 (2007).

[45] T. W. Baumgarte, *Innermost stable circular orbit of binary black holes*, Physical Review D **62**, 024018 (2000).

[46] A. Donos and J. P. Gauntlett, *Navier-Stokes equations on black hole horizons and DC thermoelectric conductivity*, Physical Review D **92**, 121901(R) (2015).

[47] S. A. Hartnoll and D. M. Hofman, *Locally Critical Resistivities from Umklapp Scattering*, Physical Review Letters **108**, 241601 (2012).

[48] L. Onsager, *Reciprocal Relations in Irreversible Processes. I.*, Physical Review **37**, 405 (1931).

[49] A. Donos and J. P. Gauntlett, *The thermoelectric properties of inhomogeneous holographic lattices*, Journal of High Energy Physics **2015**, 35 (2015).

[50] E. Banks, A. Donos, and J. P. Gauntlett, *Thermoelectric DC conductivities and Stokes flows on black hole horizons*, arXiv:1507.00234v3, 2015.

[51] G. T. Horowitz, J. E. Santos, and D. Tong, *Optical conductivity with holographic lattices*, Journal of High Energy Physics **2012**, 168 (2012).

[52] R. A. Davison, K. Schalm, and J. Zaanen, *Holographic duality and the resistivity of strange metals*, Physical Review B **89**, 245116 (2014).

[53] Y. Liu and X.-M. Wu, *Breakdown of hydrodynamics from holographic pole collision*, Journal of High Energy Physics **2022**, 155 (2022).

[54] J. Aretz, *Quasinormal Modes of Gubser-Rocha Holomatter*, Master's thesis, Leiden University, 2022.

[55] S. Dutta, A. Jain, and R. Soni, *Dyonic black hole and holography*, Journal of High Energy Physics **2013**, 60 (2013).

[56] J.-H. She, B. J. Overbosch, Y.-W. Sun, Y. Liu, K. E. Schalm, J. A. Mydosh, and J. Zaanen, *Observing the origin of superconductivity in quantum critical metals*, Physical Review B **84**, 144527 (2011).